Report for
80NSSC20M0261

Unmanned Aerial System (UAS) Research for Public Safety Applications

Task 7: Spectrum Considerations for UTM
Final Report

Program Manager: Keenan Roach
Principal Investigator: Kenny Cheung

Prepared for NASA Ames Research Center Moffett Field, California 94035

TABLE OF CONTENTS

TABLE OF FIGURES

TABLE OF TABLES

TABLE OF ACRONYMS

A2A	Air-to-Air
A2G	Air-to-Ground
AAM	Advanced Air Mobility
AI	Artificial Intelligence
AGL	Above Ground Level
BS	Base-Station
BVLOS	Beyond Visual-Line-of-Sight
CDA	Collision and detection avoidance
CL	Centralized Learning
CONOPs	Concept of Operations
COTS	Commercial Off-the-Shelf
C2	Command and Control
DDQN	Double Deep Q Network
DL	Downlink
DNN	Deep Neural Network
DQN	Deep Q Network
EE	Energy Efficiency
FAA	Federal Aviation Administration
FCC	Federal Communications Commission
FedAvg	Federated Averaging
FL	Federated Learning
G2A	Ground-to-Air
G2G	Ground-to-Ground
LTE	Long Term Evolution
LOS	Line-of-Sight
MDP	Markov Decision Process
MHz	Megahertz
ML	Machine Learning
NAA	National Aviation Authority
NAS	National Airspace System
NASA	National Aeronautics and Space Administration
NNA	Non-Networked access
NPRM	Notices of Proposed Rulemaking
NLOS	Non-Line-of-Sight
NSS	Network Supported Service
OSO	Operational Safety Objectives
PPL	Private Pilot License
pwFedAvg	Proportional Weighted Federated Averaging
PU	Primary User
PSNR	Peak Signal-to-Noise Ratio
RELU	Rectified Linear Unit
RL	Reinforcement Learning
SAS	Spectrum Access System

SDSP	Supplemental Data Service Provider
SE	Spectral Efficiency
SINR	Signal-to-Interference-plus-Noise Ratio
SSS	Spatial Spectrum Sensing
SU	Secondary User
sUAS	Small Unmanned Aircraft System
UA	Unmanned Aircraft
UAM	Urban Air Mobility
UAS	Unmanned Aircraft Systems
UAV	Unmanned Aerial Vehicle
UL	Uplink
USC	United States Code
USS	UAS Service Supplier
UTM	Unmanned Traffic Management
VLOS	Visual Line-of-Sight
V2V	Vehicle-to-Vehicle

EXECUTIVE SUMMARY

This report focuses on the spectrum considerations for Unmanned Aerial Systems (UAS) in public safety and Unmanned Aircraft System Traffic Management (UTM). As UAS usage grows in various sectors, ensuring efficient, scalable, and reliable wireless communications is crucial. This research aimed to address critical gaps in spectrum management for safe UAS operations. The goal of this research was to identify current and future spectrum needs for UAS operations, assess the availability of spectrum resources, and develop dynamic spectrum sharing solutions. The research also assessed interference challenges in unlicensed bands and proposed optimization algorithms to ensure reliable data transmission.

The research yielded several important findings. In relation to spectrum shortfalls, the research revealed that current spectrum allocations and technologies (e.g., unlicensed bands) are insufficient to meet the needs of UAS operations, especially as UAV density under BVLOS increases in the airspace. Both public safety and commercial UAS operations will face challenges unless new spectrum resources, supported by algorithmic innovations, are developed. On the topic of collaborative spectrum sensing and sharing, spectrum sensing can be used to efficiently allocate underutilized spectrum bands. Introducing *collaborative* sensing technologies can further improve accuracy. By using ML/AI-driven solutions, UAVs can autonomously detect and share underutilized spectrum resources. Additionally, when considering the optimization of communication systems, newly developed algorithms significantly enhance communication performance in interference-heavy environments. The implementation of such algorithms for video and data transmission by UAVs resulted in higher throughput and more reliable communication even with interference. Finally, a federated learning-based framework allows UAV operators to collaboratively learn from decentralized data. This approach enhances data privacy and security, while improving the accuracy and efficiency of spectrum sensing and allocation decisions across large, multi-cell environments.

Despite these advancements, several challenges regarding spectrum considerations for safe and reliable UAS operations remain. Actions are required in a number of areas. Validation of ML/AI-driven spectrum management technologies is a challenge, specifically the investment in spectrum management frameworks that can dynamically detect and allocate underutilized spectrum bands. ML/AI-driven algorithms in UAS communication systems should be experimentally tested, verified, and refined, especially in complex operations. Secondly, spectrum policy advocacy poses challenges. Collaboration with policymakers and regulatory bodies, such as the Federal Communications Commission (FCC) and National Telecommunications and Information Administration (NTIA) to ensure proper spectrum allocation for UAS operations, is paramount, especially priority access for public safety and first responders. Enhancing public safety operations with future-proof technologies is an additional challenge, including investing in advanced communication technologies (e.g., equipping UAVs with C-band radio, which is being repurposed

by the FCC in August 2024) and spectrum management tools that will enable UAS to operate reliably and efficiently in BVLOS.

1 INTRODUCTION

Unmanned aerial systems (UAS) have attracted significant interests from communications and networking, robotics, and control societies for exploring novel applications such as on-demand connectivity, search-and-rescue operations, and situational awareness, to name a few. While such efforts are essential, there are gaps in the fundamental research and experimentation of UAS platforms. It is clear that the current innovations based on the assumption of visual line-of-sight (VLOS) between an aerial vehicle and ground control station is a limiting factor. In order to truly unleash the potential of UAS, real-world and commercial deployments will most likely be in the form of beyond visual line-of-sight (BVLOS) scenarios, which in turn provide easier access to remote or hazardous areas, less human intervention, and reduced cost of operation. Yet, compared with the VLOS conditions, BVLOS carries higher safety risks since in the case of automated flights there may be no human observations, or the pilot may only be observing potential obstacles or other flying objects via a remote camera feed.

For safe operations of multiple UAS under BVLOS conditions, the Unmanned Aircraft System Traffic Management (UTM) system is under development to enable advanced UAS use-cases. Given the current state of knowledge, there is an immediate need for thorough assessment, analysis, and modeling of spectrum management frameworks for efficient, reliable, and scalable deployment of UAS under BVLOS scenarios. In this task, we provide a comprehensive assessment of the shortfalls, impact, and needed changes in spectrum management to accommodate the predicted levels of UAS operations and the diversity of technology solutions to address challenges facing low altitude operations.

1.1 Research Subtasks

This research was organized across the following inter-related subtasks.

1.1.1 Subtask 1: Evaluating the Spectrum Needs for UAS

This subtask aimed to provide an assessment of current and future spectrum needs for low altitude UAS operations, including aircraft and UTM infrastructure. In this subtask, the research team presented a methodology to estimate the total spectrum resources needed for each type of wireless communication within the UTM system. The aggregated results revealed the required spectrum as UAV density increases. This analysis is critical for understanding the scalability of current spectrum allocations and predicting future needs as UAV traffic increases. The results offer valuable data for spectrum planners and regulators to ensure efficient and reliable communication networks are available for increasingly crowded airspaces.

1.1.2 Subtask 2: Exploring the Spectrum Supplies for UAS

In this subtask, the research team surveyed existing spectrum allocation in the US to determine available, underutilized spectrum or allocated spectrum that can be repurposed for UAS needs. This subtask also explored standardization and policy-making opportunities. To assess the

available spectrum resources and related technologies (such as LTE, satellite, WiFi, etc.), the research team divided efforts into two parts for this subtask. A simulator that the research tean developed was introduced, which integrates wireless and flight simulations. This is a crucial component for evaluating the performance of various wireless communication technologies and the allocated spectrum for UAV operations. Additionally, this subtask included the investigation of policy-making initiatives focused on spectrum licensing mechanisms for UAV operations in the U.S., including efforts by the FCC and NTIA to develop a national spectrum strategy.

1.1.3 Subtask 3: Dynamic Spectrum Sensing and Access

This subtask encompassed the examination of the requirements for a dynamic spectrum access management service to assign and monitor spectrum use within UTM that supports UAS operations. A data-driven framework was proposed for collaborative wideband spectrum sensing and scheduling for networked UAVs, which act as the secondary users to opportunistically utilize detected spectrum holes. To this end, the research team proposed a multi-class classification problem for wideband spectrum sensing to detect vacant spectrum spots based on collected RF signal samples. To enhance the accuracy of the spectrum sensing module, the outputs from the multi-class classification by each individual UAV are fused at a server in the UTM ecosystem to achieve collaborative spectrum sensing. In the spectrum scheduling phase, reinforcement learning (RL) solutions were leveraged to dynamically allocate the detected spectrum holes to the secondary users (i.e., UAVs). To evaluate the proposed methods, a comprehensive simulation framework was established that generates a near-realistic synthetic dataset using MATLAB LTE toolbox by incorporating LTE base-station (BS) locations in a chosen area of interest, performing ray-tracing, and emulating the primary users channel usage in terms of I/Q samples. This evaluation methodology provides a flexible framework to generate large spectrum datasets that could be used for developing ML/AI-based spectrum management solutions for aerial devices.

1.1.4 Subtask 4: Saturation and Interference Analysis

This subtask focused on conducting saturation/interference analysis on the current spectrum used by UAS, such as the ISM band. In this subtask, the research team conducted a thorough and in-depth analysis of UAV communication systems with ground nodes under varying interference conditions, focusing on the development of transmission policies to enhance network performance in unlicensed spectrum bands. Specifically, this included modeling and mitigating the impact of interference, queuing delay, and buffer overflow on expected throughput. By employing distributed optimization algorithms, including methods like coordinate descent and consensus-based distributed optimizations to find optimal transmission policies, the subtask explores techniques for improving the efficiency of packet transmission in complex UAV-ground environments. Additionally, video streaming quality was optimized through two-step optimization algorithms that maximize metrics such as Peak Signal-to-Noise Ratio (PSNR), balancing video encoding rates and transmission policies over all nodes.

1.1.5 Subtask 5: Spectrum Management Framework for Operators

Subtask 5 proposed a data-driven framework for collaborative wideband spectrum sensing and scheduling across distributed UAV operators. The main goal of the solution is to enable distributed

model training, which in turn, provides data privacy and security. In the *model training stage*, the research team explored dataset generation in a multi-cell environment and trained a machine learning (ML) model using the federated learning (FL) architecture. Unlike the existing studies on FL for wireless that presume datasets are readily available for training, this research proposed a novel architecture that directly integrates wireless dataset generation, which involves capturing I/Q samples from over-the-air signals in a multi-cell environment, into the FL training process. In the traditional FL that employs FedAvg as the aggregating method, each UAV is assigned an equal weight during model aggregation. However, due to the disparities in channel conditions in a multi-cell environment, the FedAvg approach may not generalize effectively for all the UAV locations. To address this issue, a proportional weighted federated averaging method (pwFedAvg) was utilized, in which the aggregating weights incorporate wireless channel conditions and received signal powers at each individual UAV. As such, the proposed method integrates the intrinsic properties of wireless datasets into the FL algorithm. This subtask builds upon the results from subtask 3.

2 SUBTASK 1: EVALUATING THE SPECTRUM NEEDS FOR UAS

2.1 Introduction

The UTM architecture is being developed to orchestrate safe operation of multiple UAVs. Within the concept of operations of the UTM architecture (Kopardekar et al., 2016), the need for spectrum resources arises for the wireless communications involved between the UAV, the UAV operator and the USS network. Since UAVs operating in UTM are not assigned a particular frequency band, it is essential to know what resources are needed for safe operations especially in BVLOS conditions. Subtask 1 focuses on a methodology to provide an estimate of the aggregated spectrum resources required for each kind of wireless communication within the UTM system. The aggregated results indicate how much spectrum is necessary when the density of UAVs increases.

2.2 Methods

As shown in Figure 1, the research team followed the methodology adapted from (Kakar, 2015), to compute spectrum requirements for a given coverage cell that involves the information exchange between the UAVs, the spectrum efficiency, and the density of UAVs. To compute the total spectrum required, the formula multiplies the frequency reuse factor (K). Therefore:

$$W = \frac{K.B.M.R}{U.E}, \tag{2.1}$$

where, K is the frequency reuse factor, B is the data rate requirement (kbit/s) for a single UAV, M is the UAV density in a single cell, U is the utilization factor (≤ 1), R is the redundancy factor (≥ 1) that allows backup links, E is the spectral efficiency (bits/s/Hz). Finally, W (MHz) is the aggregate bandwidth requirement.

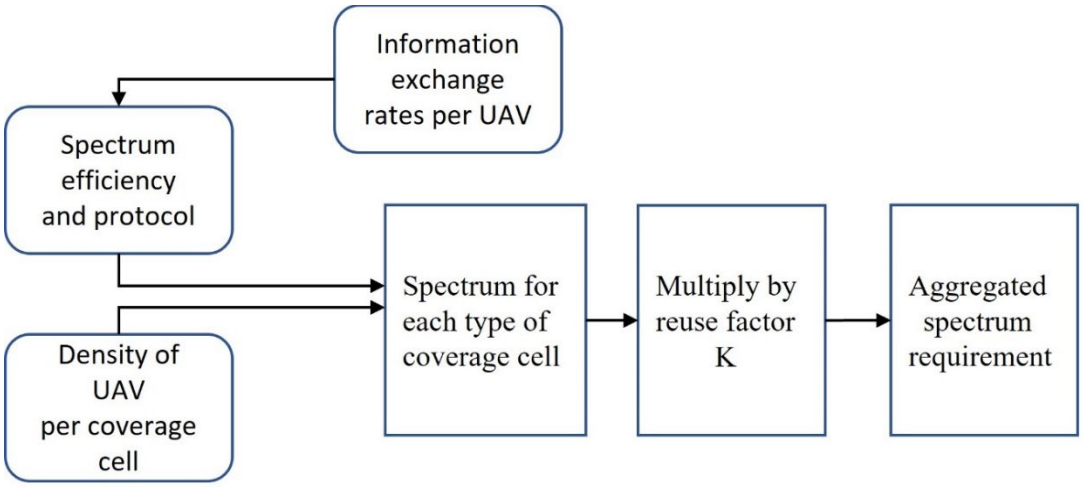

Figure 1. Methodology to compute aggregated spectrum requirements.

2.3 Results

2.3.1 Remote ID Requirements

Remote ID is the ability of a drone in flight to broadcast identification and location information that can be received by other parties. For safety and security reasons, the FAA has mandated that UAVs must broadcast Remote ID. Remote ID will provide information such as the identity, location, and altitude of the UAV and its control station or take-off location. Table 1 summarizes the required amount of data rate for broadcasting Remote ID.

Table 1. RemoteID contents of each UAV.

RemoteID Contents			
RemoteID	Bits	Min Transmission Rate (Hz)	Data rate (b/s)
UVIN	32	1	32
Latitude	32	1	32
Longitude	32	1	32
Altitude	32	1	32
Velocity	32	1	32
Latitude	32	1	32
Longitude	32	1	32
Altitude	32	1	32
Emergency Status	8	1	8
Time Status	40	1	40
Overhead	40	1	40
		Total	344

Given the contents of RemoteID data from Table 1, Table 2 computes the total spectrum required for broadcasting RemoteID when multiple UAVs are in the area using the methodology defined in Figure 1.

Table 2. Estimated aggregated spectrum requirements for broadcasting RemoteID.

Aggregating RemoteID requirements						
M	K	B (bps)	R	U	E (b/s/Hz)	W (MHz)
5	7	344	2	1	0.75	0.032107
10	7	344	2	1	0.75	0.064213
20	7	344	2	1	0.75	0.128427
50	7	344	2	1	0.75	0.321067
100	7	344	2	1	0.75	0.642133

2.3.2 Requirements for Command and Control (C2) with Video

C2 link plays a major role in delivering command and control information to the UAVs. In computing the requirements for both uplink (UL) and downlink (DL), the default values mentioned in the (ITU-R, 2009) were used. Since the requirements for UAVs flying below 400 ft are being computed, cell type A is used to determine the estimated spectrum requirements for each cell. As seen in Table 3, it can be clearly observed that as the UAV density (M) increases the total spectrum requirement increases. Note that the computations consider UAV communications with video for command and control.

Table 3. Estimated aggregated spectrum requirements for UAV communications with video for C2.

Spectrum requirements for UAV Communication with Video								
Cell Type	M	K	BR/UE (KHz)			Spectrum Needed (MHz)		
			UL	DL	Overall	UL	DL	Overall
Surface	3	1	23.1589	437.279	460.438	0.06948	1.31184	1.38131
A	5	7	23.1589	437.279	460.438	0.81056	15.3048	16.1153
A	10	7	23.1589	437.279	460.438	1.62112	30.6095	32.2306
A	20	7	23.1589	437.279	460.438	3.24224	61.2191	64.4613
A	50	7	23.1589	437.279	460.438	8.1056	153.048	161.153
A	100	7	23.1589	437.279	460.438	16.2112	306.095	322.306

2.3.3 Requirements for UAV-UAV Communication

When UAVs operate in areas where manned aircraft are more common, operators are responsible for ensuring safe separation from all other aircraft. This can be achieved through in-flight de-confliction services provided by USS, which help detect and notify operators of nearby traffic, or by using ground-based or airborne technologies such as position-sharing systems, vehicle-to-vehicle (V2V) communication, ground-based or airborne surveillance data, and collision detection and avoidance (CDA) capabilities. Table 4 captures an estimate of spectrum requirements for UAV-UAV communications, where a data rate of 200 kbps is assumed for UAV-UAV communication.

Table 4. Estimated aggregated spectrum requirements for UAV-UAV communications.

UAV-UAV Communication						
M	K	B (bps)	R	U	E (b/s/Hz)	Spectrum needed (MHz)
5	7	200000	1	1	0.75	9.33333333
10	7	200000	1	1	0.75	18.6666667
15	7	200000	1	1	0.75	28
20	7	200000	1	1	0.75	37.3333333
30	7	200000	1	1	0.75	56

3 SUBTASK 2: EXPLORING THE SPECTRUM SUPPLIES FOR UAS

3.1 Introduction

To evaluate the available spectrum supplies and the performance of corresponding technologies (such as LTE, satellite, WiFi, etc.), research efforts were divided into two parts in this subtask. First, the developed simulator that can be used for integrated wireless-flight simulation was presented. This is a critical aspect of the Task 7 research needed to be addressed to be able to evaluate the performance of various wireless communication technologies as well as allocated spectrum for UAV operations. Secondly, the research team explored the policy-making efforts that are aimed at spectrum licensing mechanism for UAV operations in the U.S. This includes the FCC and the NTIA efforts to develop a national spectrum strategy.

3.2 Developing a Simulation Framework for UAV Spectrum Studies

To evaluate and investigate various spectrum allocation and sharing for UAS, a reliable and comprehensive simulation framework is needed. Such a framework should provide the capabilities to model different subsystems of UAVs, ground control stations, and their communication links. As such, the research team initially considered MATLAB and its UAV Toolbox in Simulink for designing, simulating, testing, and deploying UAVs, but found that although MATLAB and UAV Toolbox provide a powerful simulation framework, there are some limitations, such as challenges for integrating wireless communication channel models for radio access networks. Two major requirements for a BVLOS scenario with the UAV simulator are wireless communication channel modeling between different entities and simulation of multiple UAVs in the same environment. To select a simulation framework that fit the research requirements, the research team also considered several open-source simulators. In particular, the functionalities and limitations of FlyNetSim, UTSim, Airsim, ROS+Unity were considered. After thorough investigations, the conclusion was that the existing open-source simulators have several limitations, as follows:

1) No air-to-ground wireless channel modeling,
2) Not compatible with required features according to UTM architecture,
3) Lack of mission planning functionality,
4) Not considering the underlying network traffic,
5) Not considering the interference resulted from other devices,
6) No Vehicle-to-Vehicle (V2V) communications feature.

Therefore, the research team aimed to develop a simulator that addresses the forementioned aspects as well as some additional ones. To this end, the Task 7 team set two specific goals for the simulator:

- Goal 1: To be able to model various public safety scenarios in the simulation tools.
- Goal 2: To investigate the performance of various spectrum supplies and their access/allocation policies.

To achieve these goals, the approach consisted of integrating two popular simulators, namely NS-3 and ArduPilot. This approach enabled the implementation of reference public safety scenarios in NS-3, which is a popular open-source network simulator. Furthermore, NS-3 is capable of modeling various wireless protocols (LTE, 5G, WiFi, LEO sat.).

Figure 2 shows the overall system architecture of the simulator. In this case, multiple UAVs are simulated via Ardupilot, and each UAV has a corresponding ghost node in the NS-3 simulator. Each UAV can be controlled by a UAS operator through the network. Furthermore, each UAV sends telemetry data to its UAS operator through the network.

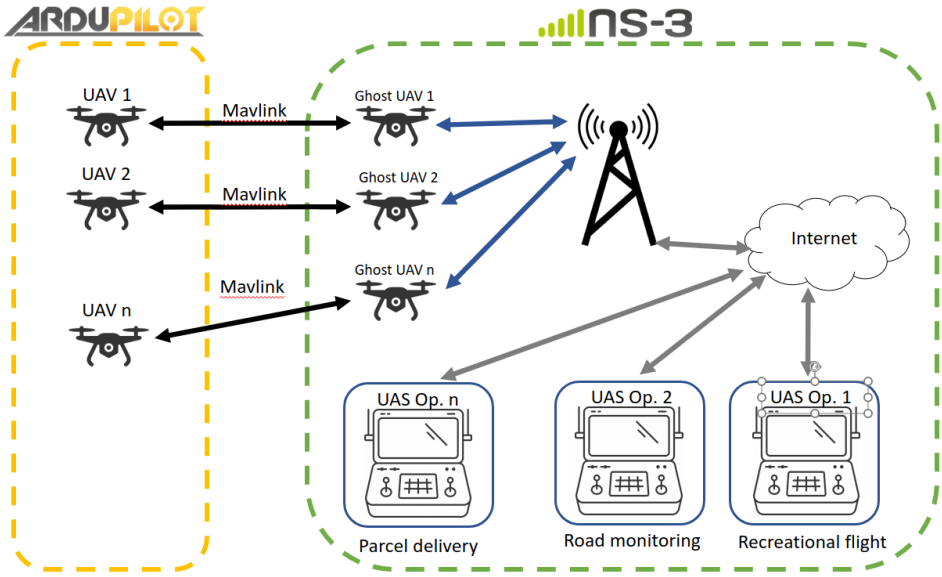

Figure 2. Overall system architecture of the simulator.

A main focus of subtask 2 consisted of cellular technology as the main spectrum supply to provide wireless communications to the UAVs. The simulator developed provides several key features:

- *Feature 1: Flexibility to define UAV operations.* UAVs can be launched from different locations and different missions can be defined using Mavlink standard structure. Furthermore, it is possible to define/assign a specific mission for each UAV such as wildfire monitoring, road monitoring, etc.
- *Feature 2: Flexibility to define the cellular network.* Given that the main focus was on cellular (LTE) technology to provide wireless links to UAVs, this simulator enables to the

user to define the LTE base stations (BS) at specific locations and heights. Furthermore, each BS can be configured independently, in terms of operating uplink/downlink frequency, allocated spectrum bandwidth, etc. For evaluation purposes, configuration information was incorporated from real LTE base stations, which can be extracted from available open sources, such as: specmap.sequence-omega.net.

- *Feature 3: Full flexibility to define the type of messages.* Each UAV is configured in terms of the type of transmitted messages, frequency of transmission, message lengths, etc. Each UAV sends telemetry info (e.g., location, velocity, battery level, etc.) to the corresponding operator through the cellular network.
- *Feature 4: Implementation for Air-to-Ground Wireless Channel Model.* 3GPP-based channel models were incorporated (from release-15 of the standard) for air-to-ground wireless communications under different scenarios, such as urban vs. rural areas.

To demonstrate the effectiveness of the developed simulator, a sample set of results is presented. To simulate a public safety scenario, the researchers modeled a wildfire in California, Los Padres National Forest, which is the third largest National Forest encompassing about 1.75 million acres. The Alisal wildfire incident occurred in 2021, and Figure 3 summarizes the key information about the incident.

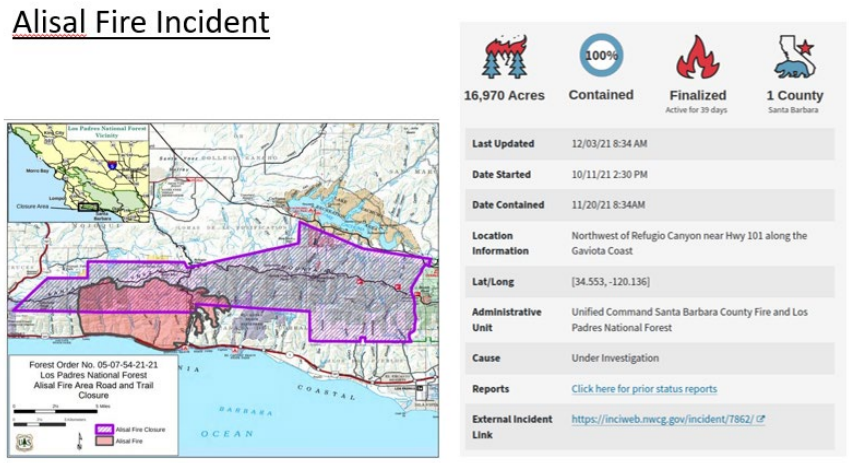

Figure 3. Alisal fire incident key details. This scenario is used to demonstrate the functionality of the simulator for UAV operation in public safety scenarios.

To establish a cellular network around the incident area, LTE base station locations were extracted from cellmapper.net website, as shown in Figure 4.

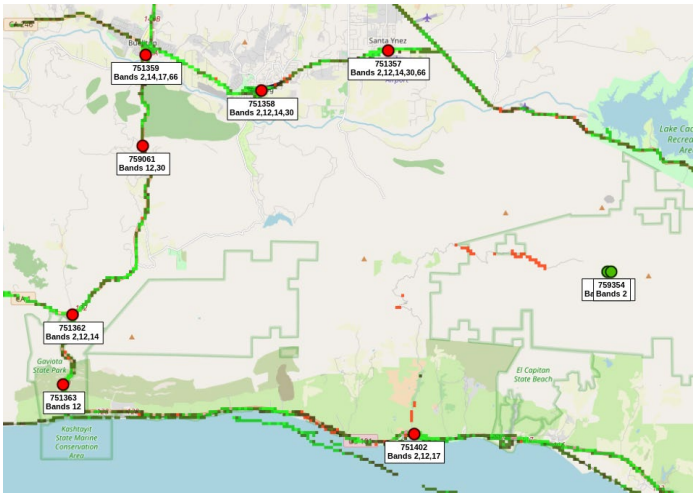

Figure 4. Location of LTE base station in the wildfire incident area.

Next, the team defined a mission path for the UAV to monitor a hill for any potential fire hazard. The UAV was sending back video streams to the GCS over the cellular network. Figure 5 shows the mission path with respect to the surrounding LTE base stations, which are denoted by blue circles.

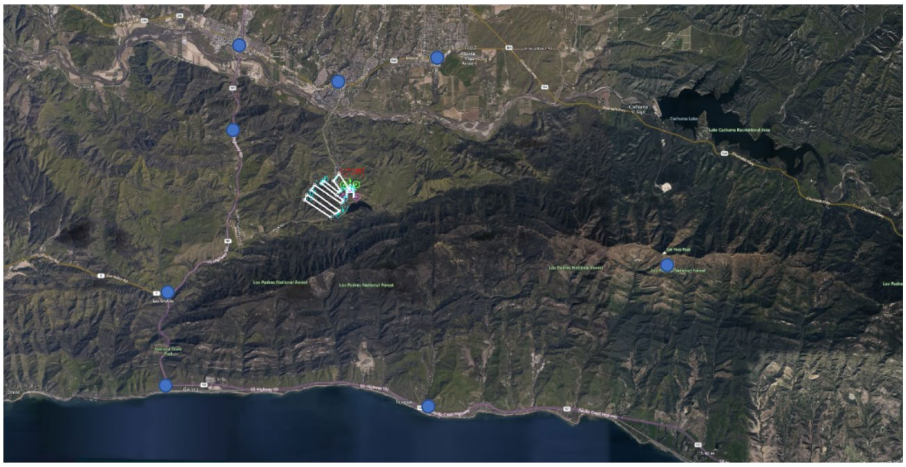

Figure 5. UAV mission path and LTE base station locations in the Alisal wildfire incident area.

Furthermore, Figure 6 shows a “zoomed-in” version of the mission path that can be defined in the simulator.

Figure 6. Defined mission path for the UAV that monitors any potential fire incidents in the Alisal area.

Once the LTE network and UAV mission were defined, the network performance was investigated as various parameters, such as spectrum operation frequency, allocated bandwidth, and video quality, etc., change. For example, Figure 7 shows the throughput performance of the streaming service as the video resolution (streamed by the UAV) is set to 1280x720 or 800x600. The LTE network is configured to operate at 700 MHz, and the allocated bandwidth is 6 MHz.

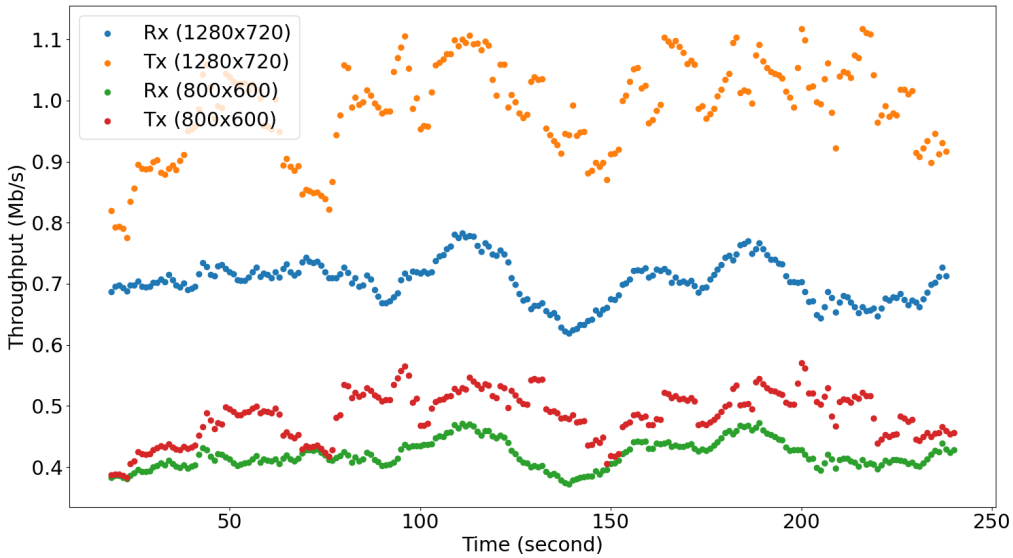

Figure 7. Throughput performance results as a function of the video resolutions.

From the results, a smaller gap between transmission and reception rates can be observed when using lower video resolutions. On the other hand, with higher resolutions, the gap increases. This suggests that a 6 MHz bandwidth allocation may not be sufficient to support such video streaming in that scenario.

In addition to the video resolution, the developed simulator allows configuration of the operating frequency band and allocated bandwidth. Figure 8shows a comparison of throughput performance for streaming 800x600 video resolution, while the allocated bandwidth is configured to be either 3 MHz or 20 MHz. The operating frequency is also either 700 MHz or 2,600 MHz.

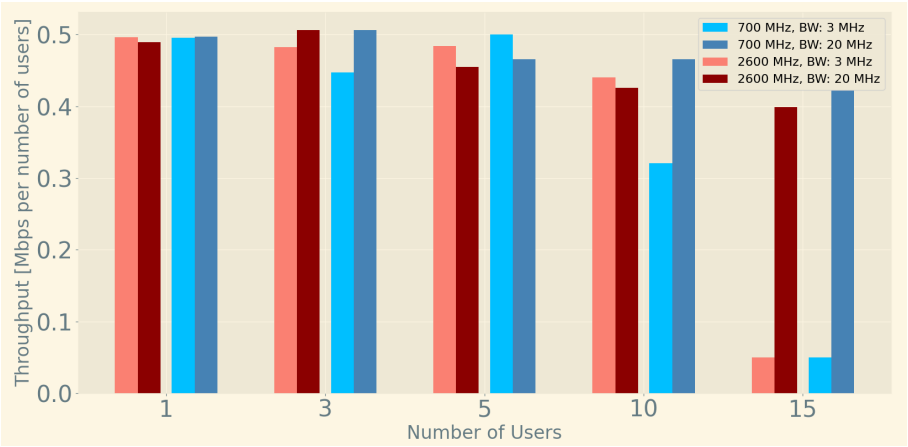

Figure 8. Throughout performance as a function of operating frequency and allocated bandwidth.

From the results, researchers observed that as the allocated bandwidth and spectrum supply increases, a greater number of users are supported simultaneously.

Overall, these results demonstrate that the developed simulator can be an effective tool to evaluate various spectrum allocation policies and investigate the performance of public safety scenarios under diverse conditions.

3.3 Policy Efforts for UAV Spectrum Allocations

Regarding the second action item, the researchers investigated ongoing policy efforts revolving around national spectrum strategy and spectrum allocations for UAV operations. The main purpose of such policy efforts is to assign licensed spectrum bands for UAV operations. BVLOS flight operations of UAVs within the national airspace (NAS) and in close proximity to people, buildings, and other aircraft inherently entail risks and require real-time monitoring by air traffic control and the pilot in command. This control and non-payload communication (CNPC) link is critical for ensuring safety and demands an interference-protected aviation-grade spectrum. Unlicensed spectrum is not viable because it lacks interference protection and is heavily used, especially in urban areas. In fact, in Subtask 4, the team investigated the impact of interference on UAV communication performance. Furthermore, while there have been significant interests in the airborne use of flexible-use spectrum and existing mobile networks, there is no licensed spectrum in the U.S. for UAV communications, leading operators to rely on unlicensed or experimental licenses without protection from harmful interference. In January 2023, the FCC issued a Notice of Proposed Rulemaking (NPRM) for spectrum rules and policies for the operation of UAS command and control in the C-band (5030 – 5091 MHz) (FCC, 2023).

Subsequently, in March 2024, the NTIA published the National Spectrum Strategy Implementation Plan that includes action items to explore repurposing this band for non-federal and commercial airborne uses (NTIA, 2024).

The goal of the FCC's NPRM was to seek comments on service rules for the C-band that will provide UAS operators with access to licensed spectrum with the reliability necessary to support safety-critical UAS communications links. The diagram in Figure 9 shows a proposed band-plan that considers two types of operations for UAS:

1) Non-Networked Access (NNA) that involves flights within a sufficiently localized area that can rely on direct wireless links between the UAS operator's controller and the UAV and therefore do not require any supporting network infrastructure. Such operations may include, for example, tower or other site inspections, public safety operations, or localized surveillance.
2) Network-Supported Service (NSS) that relies on deployed network infrastructure, such as cell towers and sites, to relay information between the operator and the UAV and may therefore extend far beyond the range of direct wireless links between operator and UAV.

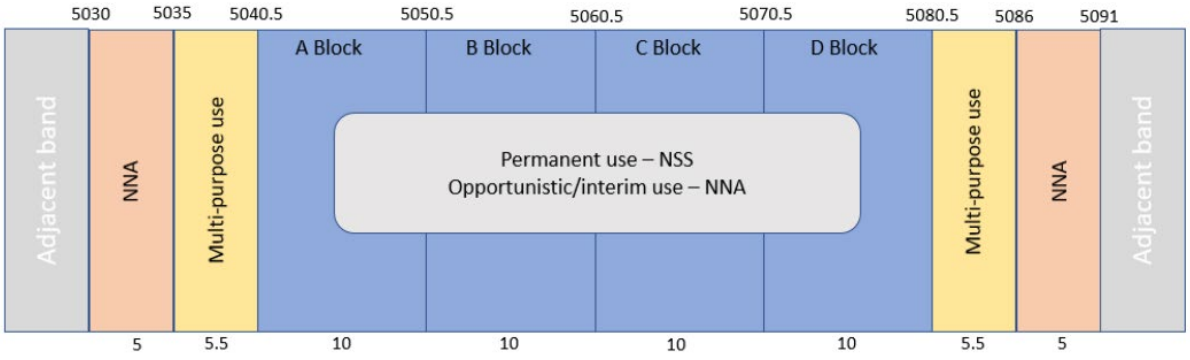

Figure 9. The envisioned band plan for 5030-5091 MHz (FCC, 2023).

In response to the NPRM, more than 70 comments from the UAS community (including Telecom companies AT&T, Verizon, T-Mobile; UAS operators; and UAS users) were submitted.

In this subtask, the researchers presented an in-depth discussion on the FCC's NPRM document, covering (i) the proposed band plan for allocating spectrum to NSS and NNA applications, (ii) a high-level overview of the dynamic frequency management system (DFMS) for this band, detailing its benefits, expected functionalities, responsibilities, and limitations, (iii) comparing the DFMS with existing frequency management systems in other bands, such as CBRS in the 3.5 GHz band, highlighting the challenges and difference, and (iv) other potential spectrum bands, such as the existing cellular and mobile networks (the so-called flexible-use spectrum bands), which can be used for UAV operations.

3.3.1 Repurposing the 5030-5091 MHz Band for UAS

The recent initiatives by the FCC and NTIA are aimed at repurposing the 5030-5091 MHz band for UAS and UTM system operations. This band is primarily allocated for Aeronautical Mobile (Route) Service (AM(R)S) and Aeronautical Mobile Service (AMS). Microwave Landing Systems are incumbents in this band, providing precision radio-based guidance to aircraft for approach and landing, especially in challenging environments where traditional Instrument Landing Systems might be inadequate. According to the NTIA and FAA, MLS installations are not widespread in the U.S. However, the Air Force uses the MLS at military bases for precision landing guidance to military aircraft. Furthermore, NASA "operates active sensor systems in the 5030-5150 MHz band on a non-interference basis" (NTIA, 2021). In addition to these incumbent users, there are other services operating in adjacent bands, including:

- Radionavigation-satellite service (RNSS) (space-to-earth) downlink at 5010-5030 MHz;
- Aeronautical mobile telemetry (AMT) downlink to support flight testing at 5091-5150 MHz;
- Aeronautical Mobile Airport Communications System (AeroMACS) in the 5000-5030 MHz and 5091-5150 MHz bands, which enables communications for surface operations in airports between aircrafts and other vehicles and assets.

3.3.2 Dynamic Frequency Management System (DFMS)

Given the scarcity of spectrum and the exponential growth of UAS operations, it is necessary to develop dynamic frequency management systems tailored for aerial operations. The U.S. has been at the forefront of developing innovative spectrum management techniques across various frequency bands such as TV White Space, the CBRS (Citizens Broadband Radio Service) in 3.5 GHz, and the 6 GHz band with Automated Frequency Coordination (AFC). However, these frameworks are not directly applicable to UAS due to several factors. For example, there is a lack of sensing frameworks for aerial systems' spectrum. In addition to authorized service parameters such as transmitted power profile and duty-cycles, it is necessary to know actual spectrum usage, either through measurements or improved data reporting. Furthermore, to improve sharing, typical deployment scenarios need to be considered. For example, the CBRS environmental sensing capabilities (ESC) that were developed to protect Navy radars will not be suitable for protecting incumbent and primary aeronautical licensees at 5030-5091 MHz. Therefore, the FCC document proposes developing a novel spectrum management solution, called dynamic frequency management system (DFMS), to improve spectrum utilization in this band.

To address the complexities of coordinating shared interference-protected access to the 5030-5091 MHz band, DFMS will be used for frequency coordination as well as providing dynamic, efficient, and automated (non-manual) access for two categories of users: NNA and NSS. The NNA services involve localized flights where the UAV communicates directly with the ground controller via wireless links, eliminating the need for network infrastructure. These operations are licensed-by-rules, which can be utilized for purposes such as public safety, localized surveillance, and tower/site inspections. On the other hand, NSS refers to network-based operations that rely on a

deployed network infrastructure for information relaying between the ground controller and UAV. The NSS operations enable services with an extended range, such as package delivery, search and rescue, mapping, etc.

The FCC proposes allocating 10 MHz of spectrum for NNA operations, 40 MHz of spectrum for NSS operations (4 licensed blocks of 10 MHz each) and making the remaining 11 MHz available for multi-purpose use by NNA or NSS licensees (FCC, 2023). Multi-purpose allocation will enable dynamic spectrum allocation and access such that the NSS licensees may receive a temporary assignment to supplement their spectrum capacity for a particular operation at a specific time and geographic location. Furthermore, the NNA users, besides having a dedicated spectrum for their operations, can opportunistically access the frequencies in a dedicated NSS block in geographic areas where the NSS licensee has not yet deployed an operating network or they do not have ongoing flight operations, thereby allowing for the opportunistic use of unused spectrum sub-bands. These coordination activities for the NSS and NNA operators will be performed with the DFMS across the entire band. The DFMS will assign time- and location-based licenses within the requested operation area and timeframe, after which the frequencies would be available in that area for assignment to another UAS operator. This will enable efficient and intensive use of the spectrum band, while providing interference-protected and reliable CNPC channels for both NNA and NSS users. Potentially, there will be multiple DFMS service providers, establishing a decentralized market structure.

In addition to the proposed band plan (Figure 9), the FCC document provides further details on (1) the scope of permissible services and eligibility conditions, (2) NNA and NSS service rules, (3) equipment authorization, (4) protection of other in-band and out-of-band services, and (5) need for international coordination (with Canada and Mexico) for near-to-border operations.

3.3.3 DFMS Requirements

To design an efficient DFMS, there are several requirements that need to be satisfied: (i) those UAS operators, who operate consistent with their assignment, should be protected from harmful interference, (ii) UAS operators should have flight authorization from the responsible parties within the UTM system (e.g., UAS service supplier (USS)), (iii) UAS operators should follow their assignment and do not cause harmful interference to other protected operations in the band and adjacent bands, and (iv) the DFMS entities should participate in decentralized markets to accommodate time- and location-based reservation requests, as well as setting associated spectrum access fees to improve spectrum utilization and avoid spectrum warehousing. Satisfying these requirements could introduce significant technical challenges that cannot be addressed using existing models. For instance, in CBRS, the spectrum access system (SAS) oversees fixed stations, enabling dynamic adjustments in transmit power or complete transmit cessation. However, unlike fixed stations, UAS operators under DFMS control cannot automatically cease operations mid-flight due to safety concerns. Additionally, dynamic frequency management approaches for the 6 GHz and TV bands rely on database queries for unlicensed access to unused spectrum sub-bands, lacking interference protection.

3.3.4 Using Flexible-Use Spectrum Bands for UAV Operations

In addition to the 5030-5091 MHz band, the FCC's NPRM document includes discussions on airborne use of flexible-use spectrum, which refers to services or spectrum bands for which the FCC's rules do not prescribe specific uses or applications. For instance, there is significant interest in utilizing existing terrestrial mobile networks (Muruganathan et al., 2021) for UAS command and control, telemetry, and payload communications due to their coverage, low latency, high throughput, and secure links. However, these networks were not designed for aerial operations, leading to potential harmful interference to adjacent licensees in nearby geographies and frequency bands. Therefore, the integration of UAS into terrestrial mobile networks may not be a seamless transition. In this study, researchers reviewed the impacts of UAS on mobile networks due to the high altitude and mobility, such that the interference impact increases with the altitude at which UAS are operating. It was concluded that the use of flexible-use spectrum by UAS can raise the risk of harmful interference on adjacent channel, adjacent band, or adjacent market operations.

4 SUBTASK 3: DYNAMIC SPECTRUM SENSING AND ACCESS

4.1 Introduction

Existing terrestrial mobile networks (e.g., 4G and 5G) provide significant wireless coverage with relatively low latency, high throughput, and low cost. This, in turn, makes the cellular network a good candidate for the operation of UAVs in BVLOS scenarios. However, the proliferation of new wireless services and the demand for higher cellular data rates have significantly exacerbated the spectrum crunch that cellular providers are already experiencing. Therefore, developing dynamic spectrum management services to sense, assign, and monitor spectrum usage within the UTM architecture is of utmost importance in order to enable advanced UAV use cases in BVLOS (Rimjha and Trani, 2021).

In this subtask, the team proposed a data-driven model for joint wideband spectrum sensing and scheduling across several UAVs, which act as secondary users (SUs) to opportunistically utilize detected spectrum holes. The proposed system model presents a unified framework that is compatible with the UTM deployment models with centralized controlling and monitoring entities (e.g., UAS service suppliers). To make development more concrete and grounded, the problem of joint spectrum sensing and sharing is formulated as an energy efficiency (EE) maximization in a wideband multi-UAV network scenario. Then, the EE optimization problem is transformed into a Markov Decision Process (MDP) to maximize the overall throughput of the SUs. To enable spectrum sensing, researchers developed a multi-label classification framework to identify vacant spectrum resources, from here on referred to as spectrum holes, based on observed I/Q samples. To enhance the accuracy of the spectrum sensing module, the outputs from the multi-label classification by each individual UAV are fused at the UTM server. In the spectrum scheduling phase, several RL algorithms are developed and implemented, including the standard Q-learning methods to dynamically allocate underutilized spectrum sub-channels to multiple UAVs. Researchers further investigated the performance of the "vanilla" deep Q-Network (DQN) and its variations, including double DQN (DDQN) and DDQN with soft-update.

Furthermore, one of the primary challenges of using machine learning (ML) methods for spectrum management is the need for large amounts of training data. The lack of available spectral data in many cases is a significant obstacle, especially for UAV networks that introduce additional complexity for large-scale experimental data collection. To address this gap, and evaluate the proposed methods, the team developed a comprehensive framework for spectrum dataset generation, which accurately models LTE waveform generation and propagation in any environment of interest for UTM-enabled UAV applications. This platform enables modeling cooperative spectrum sensing and sharing for wideband multi-UAV network scenarios and can be used for scalable generation of large spectrum datasets within an area of interest.

In summary, the key contributions of this subtask are as follows:

1) A joint spectrum sensing and access framework using raw LTE I/Q data was developed.
2) The developed spectrum sensing module identifies multiple spectrum holes in a wideband multi-channel setting.
3) RL-based techniques (i.e., DQN and its variations) were utilized to allocate the identified spectrum holes to multiple UAVs.
4) The developed solution is evaluated using realistic channel modeling between several LTE BSs and UAVs.

4.2 Methods

4.1.1.1 Network Model and Communication Protocol.

Consider a set of UAVs denoted by $\mathcal{K}$ ($|\mathcal{K}| = K$) where each UAV can perform wideband sensing over M orthogonal primary spectrum resources (sub-channels) independently. Due to the highly dynamic environment in which UAVs operate, it may not be feasible for all the UAVs to observe every vacant sub-channel. Therefore, researchers leveraged collaborative spectrum sensing by the UAVs and perform spectrum fusion at some servers located in the UTM architecture to increase the reliability of spectrum hole detection. Identified spectrum holes are allocated to the UAVs. Therefore, the overall system model is divided into two major components: (i) collaborative spectrum sensing and fusion policies, (ii) spectrum allocation and access policies.

To coordinate the spectrum sensing, fusion, and access steps, researchers assume that each time slot is divided into four consecutive sub-slots: UAV resource request ($\mathrm{t_{req}}$) , spectrum sensing (t_s), broadcasting to server (t_b), and channel access (t_a) as shown in Figure 10.

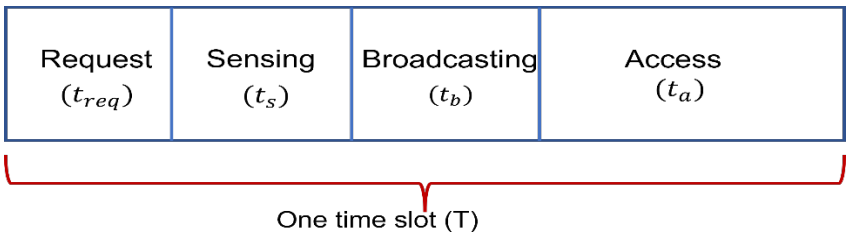

Figure 10. Time slot format.

Specifically, at the beginning of each time slot, the UAVs that require PU resources request the server for resource allocation. In the subsequent sub-slot of sensing (t_s), the UAVs perform spectrum sensing and broadcast the sensed channel information in the following sub-slot (t_b). The server then applies fusion rules and assigns spectrum holes to the requesting UAVs. The UAVs transmit on the allocated spectrum holes in the access sub-slot (t_a).

4.1.1.2 Collaborative Spectrum Sensing and Fusion Policies

Each individual UAV captures the raw I/Q samples over the air signals and predicts the availability of spectrum holes across *M* sub-channels. An associated spectrum sensing cost for each UAV k involved in sensing at time slot t is assumed. The spectrum sensing cost is the energy consumed for sensing the spectrum and is proportional to the voltage $\mathrm{V_{CC}}$ of the receiver, the system bandwidth is B, and the duration allotted for sensing is t_s (Zhang and Shin, 2012). Therefore, the spectrum sensing cost is defined as $\mathrm{SC_{km}(t)} = \mathrm{t_s V_{CC}^2 B_m}$. Upon the completion of sensing phase, the UAV k has a predicted spectrum occupancy vector $\mathbf{h_k(t)} = \left[\mathrm{h_{k,1}(t)}, \dots, \mathrm{h_{k,M}(t)}\right]$ such that $\mathrm{h_{k,m}(t)} = 0$ if the m-th sub-channel is detected vacant at time t, and $h_{k,m}(t) = 1$ otherwise. This problem can be considered as a multi-class classification problem, and the research team leveraged deep neural network (DNN) at each UAV to identify the spectrum holes and outputs the prediction vector $\mathbf{h}_k(t)$.

The server receives multiple copies of spectrum holes detected by individual UAVs and applies fusion rules that result in aggregated spectrum holes. The *n*-out-of-*K* fusion rule is defined as follows:

$$f_m(t) = \begin{cases} 0, & \sum_{k \in \mathcal{K}} \mathbb{I}\{h_{k,m}(t) = 0\} \geq n; \\ 1, & Otherwise. \end{cases} \tag{4.1}$$

where $\mathbb{I}\{.\}$ is an indicator function. In this case, $\mathbf{f}(t) = [f_1(t), \dots, f_M(t)]$ is the fused prediction of all the *M* sub-channels at the UTM server. Note that when *n=1*, the *n*-out-of-*K* rule is equivalent to the "OR" rule, and *n=K* is the same as the "AND" rule.

4.1.1.3 Collaborative Spectrum Sensing and Fusion Policies

Based on the aggregated fusion result, the server then allocates sub-channels to the requesting UAVs. The UAVs then transmit data on the sub-channels allocated to them by the server in the next time step. The transmission energy consumption is denoted by $\mathrm{AC_{km}(t)}$. The access cost is the energy consumed for data transmission and is defined as $\mathrm{AC_{km}(t)} = \mathrm{t_a P_{tx}}$, where, $\mathrm{P_{tx}}$ is the transmit power and $\mathrm{t_a}$ is the time allotted to transmission. Furthermore, the transmission utility is the amount of data transmitted on the allocated sub-channel and is defined as follows:

$$R_{k,m}(t) = \mathrm{t_a B_m} \log_2\left(1 + \mathrm{SINR_{k,m}(t)}\right), \tag{4.2}$$

where B_m is the sub-channel bandwidth allocated for data transmission and $\mathrm{SINR_{km}}$ is the signal-to-interference-plus-noise ratio observed on the link between UAV and its receiver over sub-channel m.

Since it is a delayed transmission, the UAVs transmit on the spectrum holes in the current step that are detected vacant in the previous time step. Spectrum collision occurs when the previously detected spectrum holes are no longer available at the current time step. The true state of sub-channel m is denoted by $\overline{\mathrm{f_m}}(\mathrm{t})$ is assumed. To capture this, the spectrum access collision indicator $r_{k,m}(t)$ is defined as follows:

$$r_{km}(t) = \begin{cases} 1, & \text{if } \overline{f_m}(t) = 0 \text{ and } f_m(t-1) = 0; \\ -1, & \text{if } \overline{f_m}(t) \neq 0 \text{ and } f_m(t-1) = 0; \\ 0, & \text{Otherwise.} \end{cases} \tag{4.3}$$

4.1.1.4 Joint Spectrum Sensing and Access Problem Formulation

Given the presented model, the research team cast the problem of joint spectrum sensing and access as an energy efficiency optimization for the UAVs. The overall system model of collaborative spectrum sensing and access is shown in Figure 11. The overall algorithm described is shown in Figure 12.

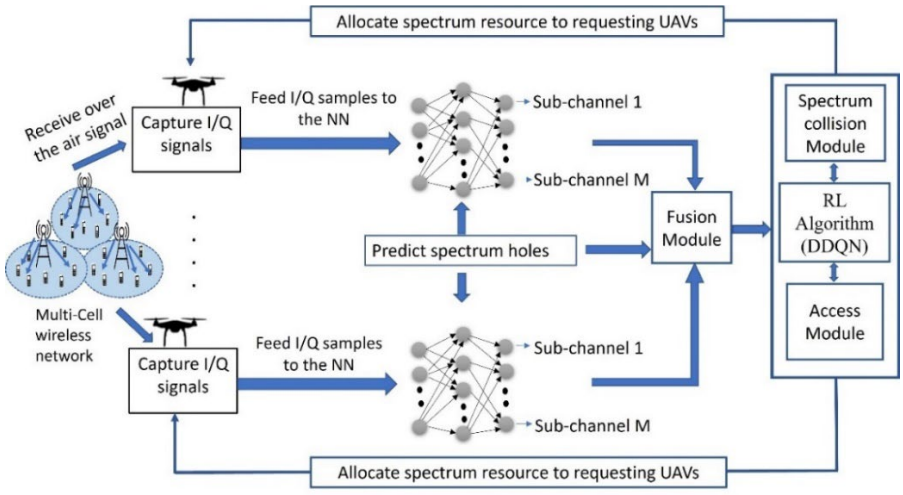

Figure 11. Proposed system model for joint spectrum sensing and spectrum scheduling.

Algorithm 1 Collaborative Spectrum Sensing and Access

Phase 1 – Spectrum Sensing and Broadcasting

1: **for** each UAV in $\mathcal{K}$ **do**
2: Capture N I/Q samples from over the air signal, where, $\mathbf{X} \in \mathbb{C}^{N\times 2}$.
3: Feed I/Q samples to the pre trained ML model that predicts the spectrum holes s.t $f : \mathbf{X} \rightarrow \mathbf{h}$.
4: Broadcast the individual spectrum hole observations $\mathbf{h} \in \{0,1\}^{1\times m}$ to the fusion center.
5: **end for**

Phase 2 – Spectrum Fusion and Access

6: Apply fusion rule to predict spectrum holes $\mathbf{f}(t)$.
7: Allocate a single spectrum hole to each requesting UAV using pre trained RL algorithm, $y_{km}(t)$, s.t. the constraints in Eq. (4) are satisfied.
8: UAVs transmit on the sub-channel allocated in the previous allocated time slot.
9: Given the spectrum allocation $y_{km}(t)$ and spectrum access collision indicator $r_{km}(t)$, compute the total utility U(t).

Figure 12. Algorithm for collaborative spectrum sensing and access.

4.2.1.1.1 Energy Efficiency Optimization

Let $y_{km}(t) = 1$ if UAV k is scheduled to use sub-channel m at time t, and $y_{km}(t) = 0$ otherwise. Given that the spectrum holes are allocated to the requesting SUs based on the sub-channel availability, sensing and access cost is incorporated to maximize the overall energy efficiency (EE) of the system. Researchers formulated the EE problem as an optimization problem as follows:

$$\begin{cases} \max\limits_{\{y_{km}(t)\}} & \mathrm{E}\{\sum\limits_{t,k,m} \dfrac{y_{km}(t) r_{km}(t) R_{km}(t)}{y_{km}(t) AC_{km}(t) + SC_{km}(t)}\} \\ \text{Subject to:} & \sum_m y_{km}(t) \le 1, \ \forall\, k = 1,2,3,\ldots\ldots K \\ & \sum_k y_{km}(t) \le 1, \ \forall\, m = 1,2,3,\ldots\ldots M \\ & \sum_{k,m} y_{km}(t) \le M - |\mathbf{f}(t)|, \\ & y_{km}(t) \in \{0,1\} \end{cases} \tag{4.4}$$

where $\mathrm{R_{km}(t)}$, $\mathrm{SC_{km}(t)}$, $\mathrm{AC_{km}(t)}$ are the amount of data transmitted, the sensing cost, and transmission cost by the SU k on sub-band m simultaneously. The constraints guarantee that each UAV is scheduled to use at most one sub-channel, while the total number of scheduled UAVs is at most equal to the number of detected spectrum holes at time t , which is $\mathrm{M} - |\mathbf{f}(\mathrm{t})|$.

The above optimization problem is a fractional integer programming problem, which is NP-hard in general. If considering the maximization of the numerator alone, which is the total utility of the UAVs over all sub-channels, the problem will become an integer programming problem. In this case, the utility would depend on the spectrum usage pattern by the PUs, which is captured by $\mathrm{r_{km}(t)}$, as well as the channel condition between the BSs and UAVs that determine the amounts of transmitted data $\mathrm{R_{km}(t)}$. To tackle this utility optimization problem, the channel occupancy

$\overline{f_m}(t)$ is modeled as a Markov process, which enables the use of a Markov decision process (MDP) formulation to solve this problem and develop a dynamic spectrum allocation policy to the SUs (Sutton and Barto, 2018).

4.2.1.1.2 Dynamic Spectrum Allocation Using RL

An assumption is that there exists M sub-channels in the system, each sub-channel can be modeled as an independent two-state Markov chain. The transition probability function **P** can then be viewed as a set of transition probability matrices $\{\mathbf{P}_i\}$ for each sub-channel that capture the randomness in the assumed multi-user multi-channel environment. Hence, researchers can formulate the total utility of the SUs into a traditional MDP which is governed by the tuple ($\mathcal{S}$, $\mathcal{A}$, $\{\mathbf{P}_i\}$, U, γ), consisting of the set of states $\mathcal{S}$, set of actions $\mathcal{A}$, a transition probability function $\{\mathbf{P}_i\}$, a reward function U, and a discount factor γ. To solve an MDP using RL, an agent learns to make decisions in an uncertain environment by maximizing a cumulative reward over a sequence of actions. Specifically, the agent interacts with an environment by taking actions that transition the system from one state to another, and the agent receives a reward that is commensurate with the merit of the action. The discount factor determines the relative importance of immediate and future rewards. One of the most popular RL methods is Q-learning (Sutton and Barto, 2018).

The classical Q-learning is table-based, i.e. the values of the Q-function are stored in a table of size $|\mathcal{S}|\times|\mathcal{A}|$. However, when the size of the state and action spaces get large, the complexity of tabular Q-learning becomes cumbersome. For example, with $M = 16$ sub-channels, the Q-table will be of size $65{,}537 \times 17$.

4.2.1.1.3 DDQN-Based Spectrum Allocation

To address the complexity issue, the deep Q-learning approach is used to approximate the Q-function by a neural network Q_θ called Double Deep Q-Network (DDQN) and train its weights θ using experience replay. As the name suggest, there are two networks when using DDQN where, Q_θ is called the primary network and Q'_θ is called the target network and the weights of the target network are updated periodically. In the original DDQN, the weights of target network are directly copied from the primary network every few episodes. In DDQN-soft, the target networks are updated using POLYAK averaging to smoothly update the weights ("soft-update") (Hasselt et al., 2016).

The input to the DDQN agent is a state $\boldsymbol{s}$ of size $1 \times M$. The output of the network is a vector of size $1 \times (M + 1)$ that contains the values of the Q-function with respect to state $\boldsymbol{s}$ and each of the $M + 1$ actions. In all the hidden layers, researchers used the rectified linear unit (ReLU) as an activation function. Given the neural networks input-output dimensions, the overall DDQN architecture and its interaction with the environment is shown in Figure 13, where the major components are a primary network, a target network, experience replay and the interaction with the environment to pick an action.

To train the DDQN agent, the experiences are initially stored in the memory using ϵ-greedy policy i.e., for a state s_t, an action a_t is taken randomly with probability ϵ_t or taken greedily with probability $1 - \epsilon_t$ from the current state of the DDQN network. Then, when there are sufficient

samples in the memory, a mini-batch of B experiences $\{(\mathbf{s}_i, \mathbf{a}_i, r_i, \mathbf{s}'_i)\}_i \in \mathcal{B}_t$ are randomly sampled from the memory for every time step t to train the neural networks. Here, $\mathcal{B}_t$ is the set of experiences currently available in the memory. Based on the mini-batch selected, the weights θ of the primary network Q_θ that minimize the loss function $L_t(\theta)$ are computed and updated.

4.1.1.5 Raw I/Q Dataset Generation

Previously, the research team described the role of DDQN in allocating spectrum holes to the SUs as such that the overall utility is maximized. However, each SU must first send in their spectrum hole detection results based on observed I/Q samples. Implementing a data-driven ML model for such wideband sensing demands large amounts of raw I/Q data.

While it is desirable to capture over-the-air raw I/Q signals using actual hardware, it is challenging to accomplish this goal due to the intricate nature of flying multiple UAVs within a specific environment for collaborative sensing implementation. Hence, the team resorted to generating synthetic datasets that accurately resemble collecting datasets via experimentation. To this end, MATLAB's LTE toolbox is used as outlined in (Chintareddy et al., 2023; Uvaydov et al., 2021) which extended the dataset generation to incorporate UAV specifics. The dataset is generated by incorporating the LTE base-stations and UAVs locations, as well as the 3D environment including buildings and vegetation for performing ray-tracing.

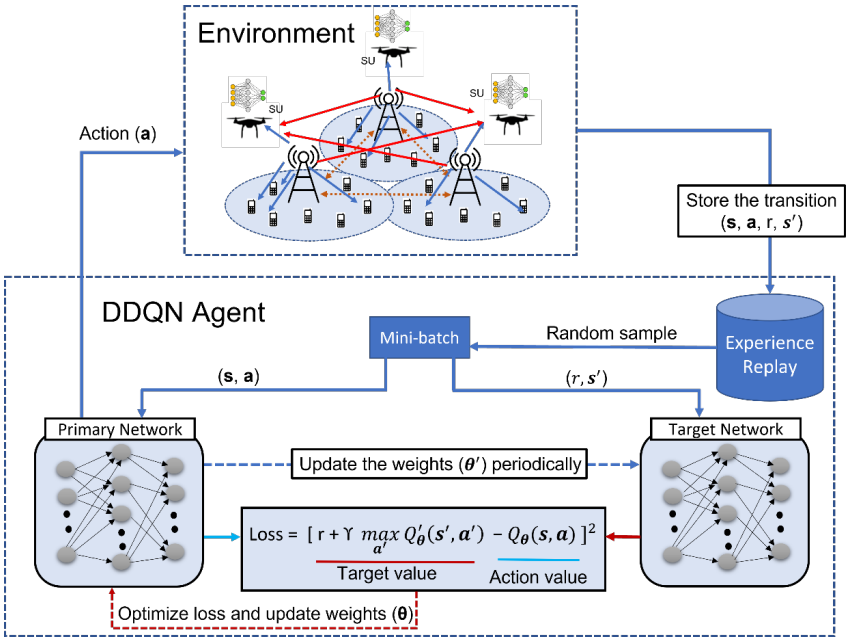

Figure 13. DDQN for spectrum allocation.

As shown in Figure 14, three neighboring cells are assumed. To perform ray-tracing experiments, the maps required are downloaded from OpenStreetMap.

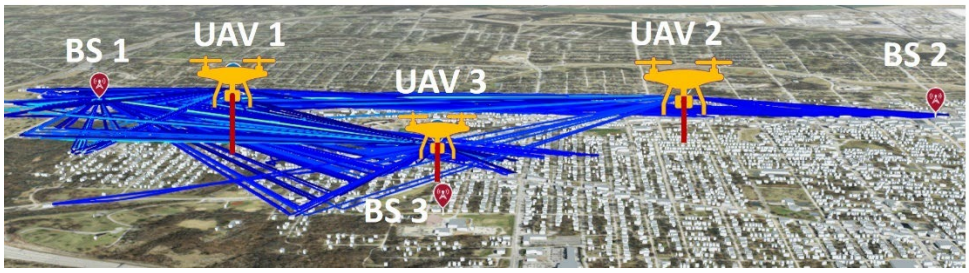

Figure 14. Ray-tracing simulation setup used for dataset generation. The plot illustrates the received signal paths at UAV location 1 from all three base-stations.

The simulation area considered is of *3* km × *3* km width with buildings and vegetation located in the Kansas City metro area. The location of the base stations is obtained from Cellmapper, an open crowd sourced cellular tower and coverage mapping service. Base-stations are defined as the transmitter sites and UAV locations as the receiver sites. Furthermore, the research team considered three UAVs and three base stations in the region of interest and use MATLAB's ray-tracer to find the channel between UAV and base-station locations. Figure 15 shows the cell-mapper tool as well as the propagation environment extracted from OpenStreetMap. Note that this scenario can be easily extended to any number of LTE cells and UAVs. It is important to emphasize that the UAVs are hovering in one location. Nevertheless, by executing the ray-tracing engine multiple times for different locations, a flight trajectory is effectively simulated.

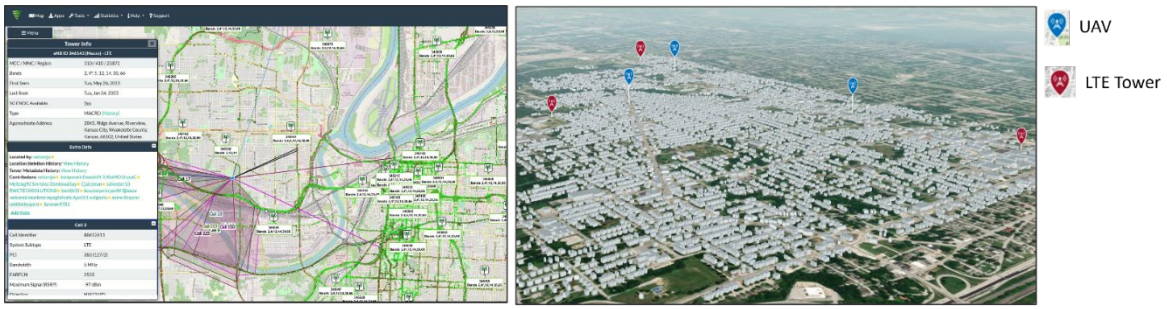

Figure 15. Extracting LTE towers configurations from Cell-Mapper open-source tool. Capturing the wireless signal propagation environment from OpenStreetMap to be used in ray-tracing.

Next, MATLAB's LTE Toolbox generates an LTE-M waveform. The entire cell bandwidth of *10* MHz (*50* resource blocks) is assumed to be split into *16* sub-channels each of size three resource blocks. In general, the base station can allocate a single sub-channel or multiple sub-channels to a PU to transfer user specific data on the downlink shared channel, and they can also use multiple access techniques for transmitting data to different PUs. However, when generating the dataset, an assumption made is that the base station partitions the bandwidth into separate sub-channels. While generating the downlink waveform of the base station, no UE specific reference signals are generated. Additionally, the broadcast channels are not corrupted with user-specific data. The appropriate indices are found and used to embed the data samples into the downlink shared

channel. As mentioned, the cell bandwidth is partitioned into *16* sub-channels, considering each combination as a label. The base station can generate 2^{16} labels, ranging from no sub-channel allocation to a fully busy cell site.

Since the research team assumed all SUs are capable of wideband sensing, each SU samples the RF signal and stores I/Q samples. The noise variance is adjusted such that the effective SINR varies from -*10* dB to *20* dB in steps of *10* dB. Since UAVs fly at an altitude, each UAV receives a signal from more than one base station which is modeled using the ray-tracing setup. The total received signal is modeled as a superposition of the signals received at each UAV as shown in Figure 14.

4.3 Results

4.3.1 Collaborative Spectrum Sensing Results

As mentioned previously, identifying spectrum holes falls into the realm of classical multi-label classification problem. Precision, Recall, and F1-score are considered as the metrics to assess the performance of such a classifier. These metrics are defined as follows:

$$\text{Precision} = \frac{\text{TP}}{\text{TP+FP}}, \quad \text{Recall} = \frac{\text{TP}}{\text{TP+FN}}, \quad F1 - score = \frac{2(\text{Precison.Recall})}{\text{Precison+Recall}}, \qquad (5)$$

where TP, FN, FP account for the number of true positives, false negatives, and false positives, respectively. To concretely capture the performance of spectrum sensing across 16 sub-channels, the micro-averages for Precision, Recall, and F1-Score are computed.

The data obtained by different UAV locations are aggregated at a central server to train a central model that can be deployed on all UAVs. For this purpose, 70% of the samples generated are used to train the DNN while the rest of samples are used for testing and validation purposes. It was observed that the performance metrics improve as the SNR improves. Specifically, for UAV locations *2* and *3*, shown in Figure 15 (a) and Figure 15 (b), the spectrum sensing performance metrics are greater than 90% for the SNR values above *10* dB. However, for UAV location 1, the overall performance metrics are worse than locations *2* and *3*. As shown in Figure 15 (a), the performance metrics are about 80 % at *10* dB SNR. This is due to weaker received signal strength in location 1, leading to noisier I/Q samples. Hence, the ML model was not able to predict the spectrum holes accurately, thereby making the rationale for exploring collaborative sensing more apparent.

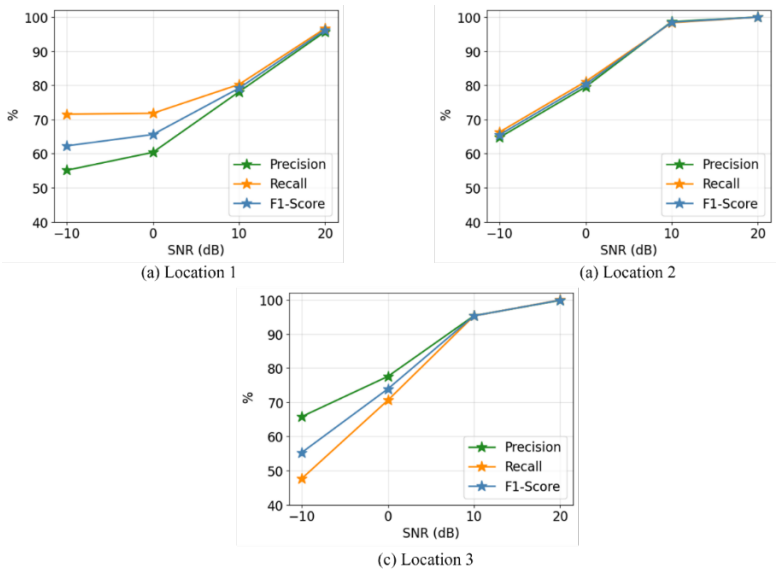

Figure 16. Performance metrics obtained at (a) Location 1, (b) Location 2, (c) Location 3.

Using spectrum fusion results, it is noted that incorporating predictions from all the UAV locations significantly improved the spectrum prediction performance at the central server. For comparison, the fusion results are shown at the central server against location *1* in Figure 16.

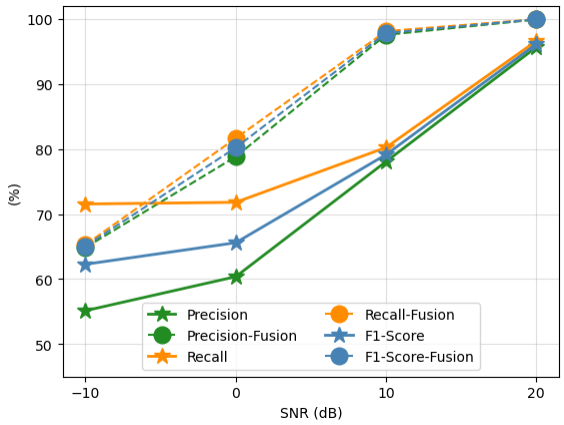

Figure 17. Comparison of F1-Score at location 1 with and without fusion.

4.3.2 Resource Allocation and Spectrum Access Results

Q-learning methods were used for allocating spectrum resources to the UAVs. In Figure 17 (a), training performance of three variants of Q-learning methods are compared for allocating a sub-channel to a single UAV whenever the fusion rule detects at least a single spectrum hole. It is observed that DDQN with soft update performs slightly better and converges earlier than DDQN and vanilla-DQN.

Next, the model is extended to allocate spectrum holes to two UAVs. In this case, the researchers have augmented the DDQN algorithm with soft update to generate two best actions. From the results in Figure 17 (b), it is observed that the utility performance with two SUs is slightly less

than two times of the performance with a single SU. It is further noted that this work explores the possibility of integrating spectrum sensing and sharing by making use of existing RL algorithms. Though Q-learning techniques were explored, different RL algorithms can be integrated into the proposed framework.

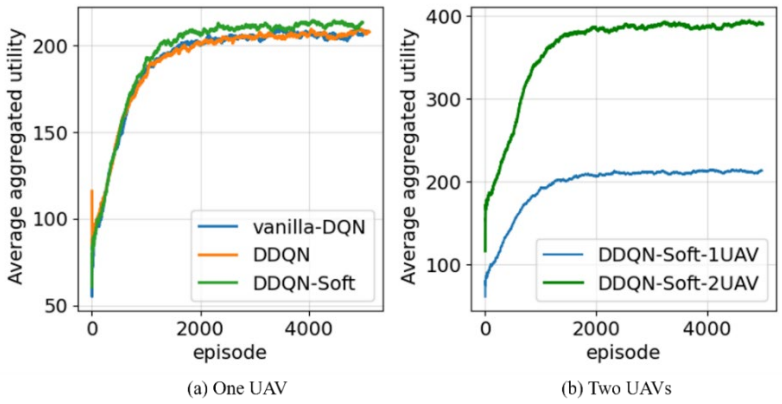

Figure 18. Training results for allocating spectrum holes to (a) one UAV, (b) two UAVs.

5 SUBTASK 4: SATURATION AND INTERFERENCE ANALYSIS

5.1 Introduction

UAVs provide excellent communication links with ground and aerial nodes, are easily deployable, and possess a high probability of establishing Line-of-Sight (LoS) communication channels. This makes them ideal for applications like video streaming in areas with limited infrastructure, disaster-affected regions or during emergency services where live video feeds are crucial for real-time decision-making (Khan et al., 2024).

UAV communications utilize both licensed and unlicensed spectrum. While licensed spectrum grants exclusive access to the channel, unlicensed spectrum, being shared, makes communication nodes more susceptible to interference from other users (FCC, 2023).This poses significant challenges for reliable and robust communication, particularly when UAVs are required to communicate delay-sensitive data, such as command-and-control (C2) information or real-time video streams. Addressing these challenges requires sophisticated transmission policies that account for interference, queuing delays, and buffer management in unlicensed spectrum bands.

In this subtask, the initial focus is on modeling the expected throughput for UAV communications in unlicensed spectrum bands such as ISM bands. A comprehensive system model was developed as shown in Figure 19 that captures the effects of interference, buffer overflow, and queuing delays. Specifically, two sources of packet loss were considered:

1) At the transmitter queue, where packets may be dropped due to buffer overflow or excessive queuing delay.

2) After transmission, where interference-related errors occur due to low Signal-to-Interference-plus-Noise Ratio (SINR).

Researchers analyzed the transmission error probability between source nodes and UAVs in the presence of interference from other nodes, accounting for both LoS and Non-LoS (NLoS) communication. By investigating Rayleigh (NLoS) and Rician (LoS) channel conditions, the team provided insights into optimizing throughput through the adjustment of channel fading thresholds (Ghazikor et al., 2023).

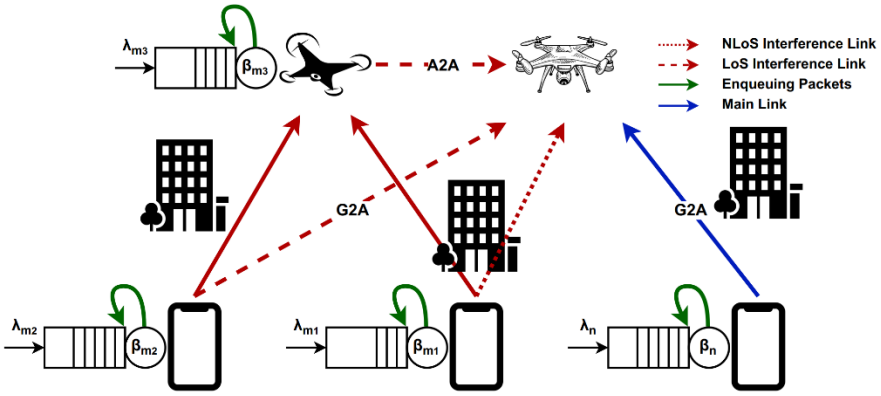

Figure 19. System model consists of ground\aerial nodes operating in unlicensed bands.

Building on the initial model, the research team then concentrated on developing distributed transmission policies for UAV networks. A framework is proposed that considers both queue and interference levels to optimize expected throughput in unlicensed spectrum bands. Two key transmission algorithms were introduced (Ghazikor et al., 2024a):

1) Interference-Aware Transmission Control (IA-TC), which optimizes the channel fading threshold for a single source node in response to interference from other ground and aerial nodes.
2) Interference-Aware Distributed Transmission Control (IA-DTC), which enables each node to adjust its channel fading threshold through consensus-based distributed optimization.

Researchers demonstrated how UAVs and ground nodes can achieve optimal transmission policies in a distributed manner, improving expected throughput in interference-prone environments.

Finally, the scope of the research was extended to address real-time video streaming over UAV networks as depicted in Figure 20, particularly in emergency and public safety applications where live video feeds are essential. In such cases, both reliable communication and high-quality video streaming are crucial. The team introduced distributed policies that jointly optimize channel fading threshold and video encoding rate to maximize Peak Signal-to-Noise Ratio (PSNR) that measures the video quality, by considering packet loss due to interference, queuing delays, and buffer overflow, as well as video distortion caused by lossy compression.

To address these challenges, two novel algorithms were proposed (Ghazikor et al., 2024b):

1) Distributed Transmission Control (DTC), which determines the optimal channel fading threshold to maximize the expected throughput across all nodes.
2) Joint Distributed Video Transmission and Encoder Control (JDVT-EC), which optimizes the video encoding rate and channel fading threshold as a transmission policy to maximize video quality, measured by PSNR, while balancing trade-offs in the packet loss and video distortions.

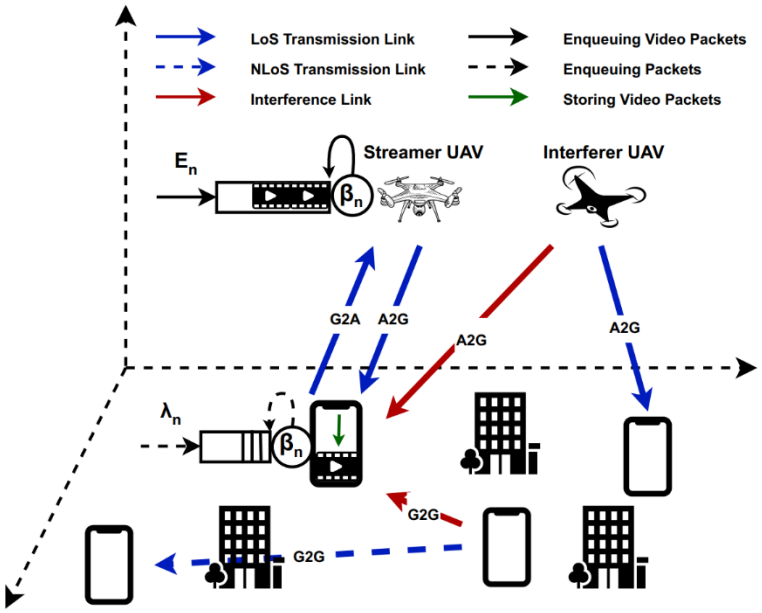

Figure 20**.** System model that includes video streaming scenario in unlicensed bands.

Through extensive simulations, the effectiveness of the algorithms in achieving optimal expected throughput and PSNR performance is demonstrated, outperforming several baseline policies. This study offers a comprehensive cross-layer framework that incorporates buffer management, interference mitigation, and video encoding control, providing a solution for UAV-enabled video streaming in unlicensed spectrum bands.

Altogether, this subtask addresses the key challenges of interference, enqueuing packets, and video encoding rate in UAV communication systems. By progressively developing models and optimization algorithms, this research contributes solutions for enhancing UAV network performance, particularly in high-demand applications like video streaming and public safety operations. The outcome of this subtask provides an optimization framework that ensures both high expected throughput for C2 packets and PSNR for experiencing higher video quality in UAV-enabled wireless communication.

5.2 Framework and Distributed Optimization Algorithms

To have a comprehensive framework, an LoS probability model was initially employed alongside a single-slope path loss model to calculate probability of establishing a LoS link and signal attenuation between ground users and UAVs (Azari et al., 2018). Accordingly, the team used an angle-based LoS probability model which is based on elevation angle, but then adopted a more

complete distance-based LoS probability model to support all channel types, including Air-to-Air (A2A), Ground-to-Air (G2A), Air-to-Ground (A2G), and Ground-to-Ground (G2G) (Kim and Lee, 2019). For all scenarios, LoS and NLoS channels were modeled using the Rician and Rayleigh distributions, respectively.

By providing channel models, an M/M/1 queue model was employed to analyze packet loss due to queuing delays and buffer overflow. This model accounted for:

1) Time threshold model: UAVs may communicate delay-sensitive data such as C2 messages. In this case, it is critical to ensure that data packets are delivered to their intended destination in a specified timeout value. Accordingly, if the source node is unable to transmit packets due to poor channel conditions (e.g., low SINR), any packet with a waiting time greater than a time threshold is discarded (Guan et al., 2016). Therefore, the probability of packet drop is given by:

2) $$P_n^{dly}(\beta_n) = Pb(T_n > T_n^{th}) = exp\left(-\left(\frac{\mu_n(\beta_n)}{T_{slt}} - \lambda_n\right)T_n^{th}\right). \quad (5.1)$$

2) Buffer overflow model: In addition to time threshold model that captures time-sensitivity of data traffics, assume that queues have limited buffer sizes as well. Therefore, there are chances that new packet arrivals are inadmissible due to buffer overflow, and thus they are dropped (Ghazikor et al., 2023) with probability:

$$P_n^{ov}(\beta_n) \approx \sum_{i=0}^{\infty} \overline{P_{i,i+1}}\pi_i = \frac{\left(1-\rho_n(\beta_n)\right)\exp\left(-B_n\eta_n\left(1-\rho_n(\beta_n)\right)\right)}{1-\rho_n(\beta_n)\exp\left(-B_n\eta_n\left(1-\rho_n(\beta_n)\right)\right)}. \quad (5.2)$$

As indicated in Eqs. (5.1) and (5.2), closed-form expressions were derived to calculate the probabilities of these two packet loss events.

Interference modeling was first done using Gamma distribution with SINR to quantify the quality of the communication link (Guan et al., 2016). Then, the interference model was refined using log-normal distribution, which better represents real-world interference scenarios (Tian et al., 2016). Using the interference model, the outage probability represented in Eq. (5.3) was calculated as the probability that the SINR falls below a threshold, resulting in packet transmission error. Researchers call this event an outage that has the following probability:

$$P_n^{out}(\beta) = Pb(\gamma_n < \gamma_{th}) = \int_{\beta_n}^{\infty} Pb\left(\tilde{h}_n^f = x\right) v_n\left(\frac{P_n\left(\hat{h}_n^f\right)^2}{\gamma_{th}}x^2 - \sigma^2, \beta_{-n}\right)dx\,. \quad (5.3)$$

Closed-form expressions for the outage probability were developed as indicated above, allowing computation of the overall packet loss by combining the time threshold, buffer overflow, and outage probabilities.

Altogether, the expected throughput was calculated by combining the three packet loss probabilities (time threshold, buffer overflow, and outage probability) as follows (Ghazikor et al., 2023):

$$R_n(\beta) = \lambda_n[1 - P_n^{lss}(\beta)] \approx \lambda_n\left[1 - P_n^{dly}(\beta_n) - P_n^{ov}(\beta_n) - P_n^{out}(\beta)\right]. \quad (5.4)$$

The expected throughput measure was used to assess the performance of UAV communication systems operating in unlicensed spectrum bands. Accordingly, two algorithms for optimizing the expected throughput were developed (Ghazikor et al., 2024a).

5.2.1 Interference-Aware Transmission Control (IA-TC)

This algorithm focuses on maximizing the expected throughput for the source node as indicated in Figure 21. This uses a coordinate descent algorithm to iteratively adjust the channel fading threshold to achieve optimal throughput only for the source node. At each step, it updates the channel fading threshold to maximize the expected throughput. Specifically, the algorithm optimizes the channel fading thresholds for the interferer nodes and the source node. The algorithm uses a coordinate descent approach, where the channel fading thresholds for the interferer nodes including Rayleigh interferers and Rician interferers and the source node are considered as three coordinate axes. Initially, the channel fading threshold for the source node and Rayleigh interferer are set as fixed parameters, and the Rician interferer threshold is varied by a step size to identify the best expected throughput in the specified coordinate. Then, the same procedure is repeated, alternating between the channel fading thresholds, allowing the algorithm to adjust each channel fading threshold iteratively until it converges to an optimal solution that maximizes the expected throughput.

Importantly, the IA-TC algorithm constantly tries to increase the channel fading thresholds for the interferer nodes until it reaches a maximum expected throughput, as the interferer nodes send fewer packets and the level of interference on the main link decreases. Furthermore, as the source node's channel fading threshold increases, the source node enqueues more packets. Thus, while packet loss in the queue rises, packet loss due to transmission error decreases. As the number of iterations of the IA-TC algorithm increases, the channel fading thresholds for the interferer nodes increase, and the source node's channel fading threshold decreases. Therefore, the source node has more transmission opportunities, while the transmission attempts by the interferer nodes are reduced.

Algorithm 1 Interference-Aware Transmission Control (IA-TC)

function IA-TC($\boldsymbol{\beta}^{ini}$, β_{max}^{Rice}, β_{max}^{Ray}, $\boldsymbol{stp}_i$, $maxiter$)
  $\boldsymbol{\beta} \leftarrow \boldsymbol{\beta}^{ini}$, $R_n^{best} \leftarrow R_n(\boldsymbol{\beta})$
  for $iter$ **in range** $maxiter$ **do**
    $R_n^{prev} \leftarrow R_n^{best}$
    if $\exists$ Rice $\in \boldsymbol{m}$ **and** $\beta_m^{Rice} + stp_m < \beta_{max}^{Rice}$ **then**
      $\boldsymbol{\beta}, R_n^{best} = CS(\boldsymbol{\beta}_m, stp_m, R_n^{best}, \beta_n)$
    end if
    if $\exists$ Ray $\in \boldsymbol{m}$ **and** $\beta_m^{Ray} + stp_m < \beta_{max}^{Ray}$ **then**
      $\boldsymbol{\beta}, R_n^{best} = CS(\boldsymbol{\beta}_m, stp_m, R_n^{best}, \beta_n)$
    end if
    $\boldsymbol{\beta}, R_n^{best} = CS(\beta_n, stp_n, R_n^{best}, \boldsymbol{\beta}_m)$
    if $|R_n^{prev} - R_n^{best}| < \epsilon$ **then**
      break
    end if
  end for
  return $\boldsymbol{\beta}, R_n^{best}$
end function

Figure 21. Interference-aware transmission control (IA-TC) algorithm.

5.2.2 Interference-Aware Distributed Transmission Control (IA-DTC)

Figure 22 shows the IA-DTC algorithm. The objective of this algorithm is to implement a distributed transmission policy that maximizes the expected throughput across all links, while recognizing that each link could potentially serve as the main link. Unlike IA-TC algorithm, increasing the channel fading threshold for interferer nodes is no longer optimal because any interferer node could also act as a main link. In this case, nodes must coordinate to converge on a transmission policy that benefits all nodes, rather than just one. To achieve this, consensus-based distributed optimization is employed (Berahas et al., 2019), where multiple nodes collaborate to reach a consensus on the optimal channel fading threshold. Each node uses its local information and objective function to iteratively communicate with its neighbors, working together to find the optimal channel fading threshold and maximize the overall expected throughput.

In this algorithm, the goal is to determine the optimal set of channel fading thresholds for all nodes. Initially, all nodes are set to their maximum channel fading thresholds, allowing each node to selfishly identify its best channel fading threshold based on the results from the IA-TC algorithm. During each iteration, if the difference between the updated channel fading threshold and the previous one exceeds a tolerance level, nodes exchange information with each other to collaboratively refine their channel fading thresholds and ultimately converge on the optimal value. Moreover, the Local Coordinate Search (LCS) function determines the best channel fading threshold for each node while having access to the channel fading thresholds of the interferer nodes. This function explores a coordinate until it identifies the optimal value that yields the highest expected throughput for the node.

Algorithm 2 Interference-Aware Distributed Transmission Control (IA-DTC)

function IA-DTC($\boldsymbol{\beta}^{max}$, $\hat{\boldsymbol{m}}$, stp, $maxiter$)
  $\boldsymbol{m}^{prev} \leftarrow \hat{\boldsymbol{m}}$, $\boldsymbol{\beta} \leftarrow \boldsymbol{\beta}^{max}$
  for n **in range** $\hat{m}$ **do**
    $\beta_n \leftarrow \boldsymbol{\beta}[n]$, $\boldsymbol{m} \leftarrow \hat{\boldsymbol{m}} - \{n\}$
    $\beta_n^{best} = LCS(maxiter, stp, \beta_n, \boldsymbol{\beta}_m)$
    $\boldsymbol{\beta}^{can}[n] \leftarrow \beta_n^{best}$, $\hat{\boldsymbol{m}} \leftarrow \boldsymbol{m}^{prev}$
  end for
  for $iter$ **in range** $maxiter$ **do**
    $\boldsymbol{\beta} \leftarrow \boldsymbol{\beta}^{can}$
    for n **in range** $\hat{m}$ **do**
      $\beta_n \leftarrow \boldsymbol{\beta}[n]$, $\boldsymbol{m} \leftarrow \hat{\boldsymbol{m}} - \{n\}$
      $\boldsymbol{R}[iter][n] \leftarrow R_n(\beta_n, \boldsymbol{\beta}_m)$
      $\beta_n^{best} = LCS(maxiter, stp, \beta_n, \boldsymbol{\beta}_m)$
      $\boldsymbol{\beta}^{can}[n] \leftarrow \beta_n^{best}$, $\hat{\boldsymbol{m}} \leftarrow \boldsymbol{m}^{prev}$
    end for
    if $|\boldsymbol{\beta} - \boldsymbol{\beta}^{can}| < \epsilon$ **then**
      $\boldsymbol{\beta}^{\star} \leftarrow \boldsymbol{\beta}^{can}$
      break
    end if
  end for
  return $\boldsymbol{\beta}^{\star}$, $\boldsymbol{R}$
end function

Figure 22**.** Interference-aware distributed transmission control (IA-DTC) algorithm.

In addition to the expected throughput maximization, researchers introduced video quality optimization by considering overall video distortion due to both lossy video compression distortion and packet loss distortion as follows (Tian et al., 2016):

$$D_n(E_n, \beta) = D_n^{cmp}(E_n) + D_n^{lss}(\beta) = D_0 + \frac{\theta_0}{E_n - E_0} + s_n P_n^{lss}(\beta). \tag{5.5}$$

The key metric for video quality is PSNR, which was formulated based on the overall video distortion in Eq. (5.6) by incorporating the channel fading threshold and video encoding rate (Ghazikor et al., 2024b):

$$\mathcal{P}_n(E_n, \beta) = 10\, log_{10}\left(\frac{(2^p - 1)^2}{D_n(E_n, \beta)}\right). \tag{5.6}$$

Correspondingly, researchers proposed the Joint Distributed Video Transmission and Encoder Control (JDVT-EC) algorithm shown in Figure 23. The goal is to maximize the average PSNR for streamer nodes in the environment by optimizing two key parameters: the video encoding rate and the channel fading threshold for each node. The optimization problem is divided into two sub-problems, where each parameter is solved individually.

At each iteration, the JDVT-EC algorithm identifies the optimal channel fading threshold and the optimal video encoding rate using the DVTC and DVEC sub-algorithms, respectively. It then compares these optimal values with the previous channel fading threshold and video encoding rate. If the difference between the current and previous values is smaller than a predefined threshold,

the algorithm returns the optimal values. The algorithm also includes a counter that tracks the number of iterations, and it terminates if a maximum iteration limit is reached.

Algorithm 2 Joint Distributed Video Transmission and Encoder Control (JDVT-EC)

function JDVT-EC($\mathbf{E}^{ini}$, $\boldsymbol{\beta}^{ini}$, $\hat{\boldsymbol{m}}$, $\boldsymbol{stp}$, itr, $\boldsymbol{\beta}^{max}$)
  $\mathbf{E}^{\star} \leftarrow \mathbf{E}^{ini}$, $\boldsymbol{\beta}^{\star} \leftarrow \boldsymbol{\beta}^{ini}$
  for ctr **in range** itr **do** $\mathbf{E}^{prv} \leftarrow \mathbf{E}^{\star}$, $\boldsymbol{\beta}^{prv} \leftarrow \boldsymbol{\beta}^{\star}$
    $\boldsymbol{\beta}^{\star} \leftarrow \text{DVTC}(\mathbf{E}^{\star}, \boldsymbol{\beta}^{\star}, \hat{\boldsymbol{m}}, \boldsymbol{stp}, itr, ctr, \boldsymbol{\beta}^{max})$
    $\mathbf{E}^{\star} \leftarrow \text{DVEC}(\mathbf{E}^{\star}, \boldsymbol{\beta}^{\star}, \hat{\boldsymbol{m}}, \boldsymbol{stp}, ctr)$
    if $|\boldsymbol{\beta}^{prv} - \boldsymbol{\beta}^{\star}| < \epsilon$ **and** $|\mathbf{E}^{prv} - \mathbf{E}^{\star}| < \epsilon$ **then**
      break
    end if
  end for
  return $\mathbf{E}^{\star}$, $\boldsymbol{\beta}^{\star}$
end function

Figure 23. Joint distributed video transmission and encoder control (JDVT-EC) algorithm.

As mentioned, the JDVT-EC algorithm involved a two-step optimization process (Ghazikor et al., 2024b).

5.2.3 Distributed Video Transmission Control (DVTC)

In this algorithm shown in Figure 24, distributed communication nodes collaborate to achieve an optimal distributed transmission strategy that benefits all nodes, if each link can serve as a main link. All nodes work together to reach a consensus on the channel fading threshold set, while they keep the video encoding rate constant. Each node processes its local information and communicates iteratively with its neighboring nodes to determine the optimal channel fading threshold. DVTC algorithm aims to determine the optimal fading threshold for all nodes. In each iteration, if the difference between the updated channel fading threshold set and the previous one exceeds a specified tolerance, the nodes exchange information about their channel fading thresholds to recalculate the optimal set.

Algorithm 3 Distributed Video Transmission Control (DVTC)

function DVTC($\mathbf{E}^\star$, $\boldsymbol{\beta}^\star$, $\hat{\boldsymbol{m}}$, $\boldsymbol{stp}$, itr, ctr, $\boldsymbol{\beta}^{max}$)
  $\boldsymbol{m}^{prv} \leftarrow \hat{\boldsymbol{m}}$
  for i **in range** itr **do** $\boldsymbol{\beta} \leftarrow \boldsymbol{\beta}^\star$
    for n **in range** $\hat{\boldsymbol{m}}$ **do**
      $\mathrm{E}_n \leftarrow \mathbf{E}^\star[n]$, $\beta_n \leftarrow \boldsymbol{\beta}[n]$, $\boldsymbol{m} \leftarrow \hat{\boldsymbol{m}} - \{n\}$
      $bst \leftarrow \boldsymbol{\mathcal{P}}[2ctr][i][n] \leftarrow \mathcal{P}_n(\mathrm{E}_n, \boldsymbol{\beta})$
      $\boldsymbol{\beta}^\star[n] \leftarrow \mathrm{LCS}(\mathrm{E}_n, \boldsymbol{\beta}, \boldsymbol{stp}, bst, \boldsymbol{\beta}^{max}, 0)$
      $\hat{\boldsymbol{m}} \leftarrow \boldsymbol{m}^{prv}$
    end for
    if $|\boldsymbol{\beta} - \boldsymbol{\beta}^\star| < \epsilon$ **then**
      break
    end if
  end for
  return $\boldsymbol{\beta}^\star$
end function

Figure 24**.** Distributed video transmission control (DVTC) algorithm.

5.2.4 Distributed Video Encoder Control (DVEC)

This algorithm illustrated in Figure 25 aims to find the optimal video encoding rates for streamer nodes using the LCS algorithm. Unlike the DVTC algorithm, each source node's video encoding rate does not affect the video encoding rates of other nodes. Thus, the video encoding rates do not need to be determined iteratively. In this algorithm, each node can be a source node and find its optimal values independently, storing it in the optimal video encoding rate set. Finally, the algorithm returns the optimal video encoding rates, which are used in conjunction with the channel fading thresholds in the JDVT-EC algorithm.

The LCS is developed to find the optimal values for each node at each iteration. In this process, a switch is used to select the decision variable including channel fading threshold and video encoding rate, while flags manage the search direction, step size, and stopping criteria. The step parameters consist of two key elements: the step divider, which adjusts the step size proportionally during the search, and the step accuracy, which controls the precision of the decision variable and stops the algorithm once the step size reaches a desired threshold. These parameters ensure that the algorithm effectively refines the decision variables while maintaining control over accuracy and efficiency. Detailed algorithm implementation is provided in a research paper (Ghazikor et al., 2024b).

Algorithm 4 Distributed Video Encoder Control (DVEC)

function DVEC($\mathbf{E}^\star$, $\boldsymbol{\beta}^\star$, $\hat{\boldsymbol{m}}$, $\boldsymbol{stp}$, ctr)
  $\boldsymbol{m}^{prv} \leftarrow \hat{\boldsymbol{m}}$, $\boldsymbol{\beta} \leftarrow \boldsymbol{\beta}^\star$
  for n **in range** $\hat{\boldsymbol{m}}$ **do**
    $\mathrm{E}_n \leftarrow \mathbf{E}^\star[n]$, $\beta_n \leftarrow \boldsymbol{\beta}[n]$, $\boldsymbol{m} \leftarrow \hat{\boldsymbol{m}} - \{n\}$
    $bst \leftarrow \boldsymbol{\mathcal{P}}[2ctr+1][0][n] \leftarrow \mathcal{P}_n(\mathrm{E}_n, \boldsymbol{\beta})$
    $\mathbf{E}^\star[n] \leftarrow \mathrm{LCS}(\mathrm{E}_n, \boldsymbol{\beta}, \boldsymbol{stp}, bst, \mathbf{0}, 1)$
    $\hat{\boldsymbol{m}} \leftarrow \boldsymbol{m}^{prv}$
  end for
  return $\mathbf{E}^\star$
end function

Figure 25. Distributed video encoder control (DVEC) algorithm.

In conclusion, in this subtask, the team initially computed the overall packet loss probability by combining time threshold model due to queuing delays, buffer overflow model due to limited buffer capacity, and outage model due to interference. These packet loss probabilities were used to calculate the expected throughput, providing a comprehensive metric to assess the performance of UAV communication systems under different interference and queuing conditions. Then, the overall packet loss also contributed to the calculation of PSNR, enabling a cross-layer analysis for video streaming optimization in the presence of interference. Ultimately, optimization algorithms were developed to maximize the expected throughput and PSNR under different scenarios.

5.3 Numerical Results

In evaluations, it was examined that the performance of the proposed framework and optimization algorithms across various setups by adjusting multiple parameters to observe their impact on UAV communications.

In the first setup, researchers assessed a scenario involving one UAV and several ground nodes, where the main communication link was between one ground node and the UAV, with other ground nodes acting as interferers. All nodes were distributed according to a Poisson distribution. The research team evaluated the expected throughput by varying the channel fading threshold for both the source and interferer nodes, demonstrating how changes in the fading threshold affect performance. Additionally, the impact of transmission power and the number of interferer nodes on expected throughput were explored. Then, the outage probability was evaluated for different SINR thresholds and number of interferers. Finally, researchers illustrated the packet loss probability in the queue as a function of time slot duration and channel fading threshold as indicated in Figure 26.

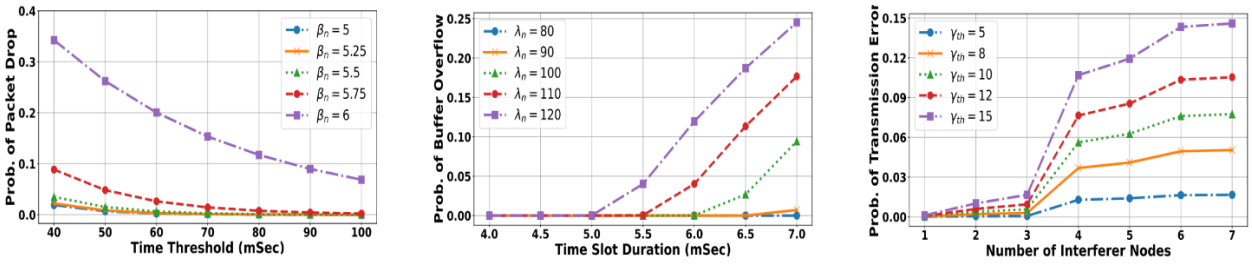

Figure 26**.** Behavior of different packet loss probabilities.

With these evaluations, researchers numerically analyzed the effects of key parameters such as transmission power and node density on the expected throughput and overall UAV communication performance in the presence of interference.

In the second setup, the performance of two proposed optimization algorithms was evaluated: IA-TC and IA-DTC. In this configuration, 10 nodes were considered, consisting of one main UAV, an interferer UAV, and 8 ground nodes. The main communication link was established between a source node and the main UAV, while other ground nodes acted as interferers communicating with the interferer UAV. For the IA-TC algorithm in Figure 27, researchers examined how changing the altitude of the interferer UAV impacted the channel fading threshold and expected throughput for the source node over IA-TC iterations.

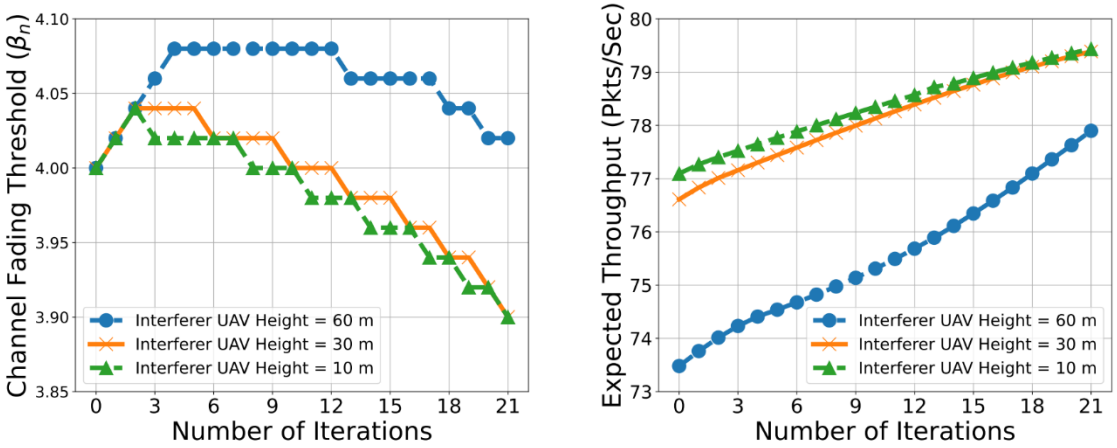

Figure 27**.** Fading threshold and throughput for the source node by IA-TC.

For the IA-DTC algorithm, researchers varied the number of nodes and SINR thresholds to observe how the optimal fading threshold changed for the main link. The results of the algorithms with different baseline policies were compared, including:

- Random policy: nodes select their channel fading thresholds randomly between zero and the upper bound.
- Aggressive policy: nodes aim to minimize packet loss from queues due to buffer overflow or time threshold by encouraging packet transmission even under poor channel conditions, potentially increasing interference.

- Selfish policy: nodes operate independently by finding selfish channel fading threshold and treating other nodes as sources of interference without coordination, which can lead to suboptimal performance.
- Conservative policy: nodes set their channel fading thresholds close to the upper bound to minimize outage probability, reducing packet loss from transmission errors but potentially increasing packet loss in the queue due to buffer overflow or time threshold.

The results are shown in Figure 28, which demonstrate the performance gains of the method. The numerical results confirmed that both IA-TC and IA-DTC consistently achieved optimal solutions.

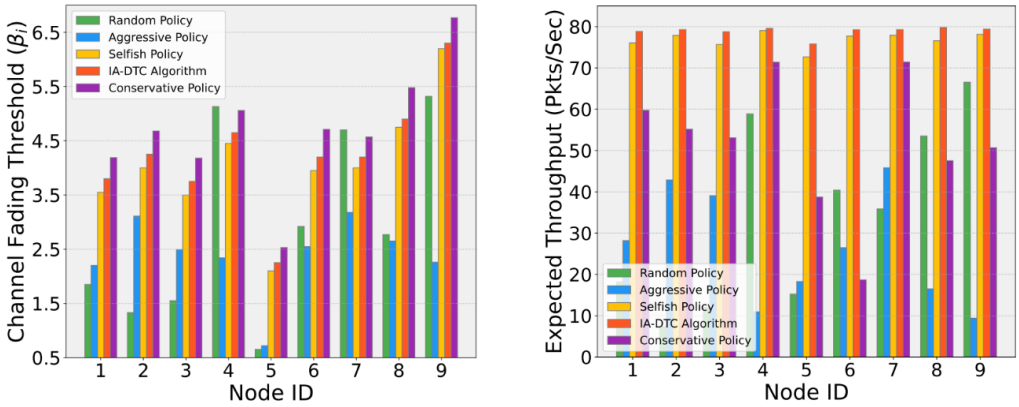

Figure 28. Fading threshold and throughput for different policies by IA-DTC.

The third step involved expanding the analysis to include a more complex network with 10 ground and aerial nodes. The key simulation parameters are summarized in Table 5.

Table 5. Key simulation parameters for video streaming setup.

Definition	Notation & Value
Communication Area	$100 \times 100\,\mathrm{m}^2$
Environmental Parameters	$\zeta = 20$, $v = 3 \times 10^{-4}$, $\mu = 0.5$
Path Loss Exponent	$\alpha_L = 2$, $\alpha_N = 3.5$
Reference Distance	$d_0 = 10$ m
Number of Sub-Channels	$\lvert\boldsymbol{F}\rvert = 14$
Rician Factor	$K_L = 15$, $K_N = 1$
Time Threshold	$T_n^{th} = 80$ ms
Time Slot Duration	$T_n^{slt} = 5$ ms
Normalized Buffer Capacity	$b_n = 100$
Transmission Power	$P_n = 0.2$ W
SINR Threshold	$\gamma_{th} = 10$
Operating Frequency	$f = 2.4$ GHz
Noise Temperature	$T = 290$ K
Bandwidth	$W = 100$ MHz
Boltzmann Constant	$k = 1.38 \times 10^{-23}$ J/K
Sensitivity Parameter	$s_n = 30$
Average Video Packet Length	$L_n = 3.04$ Kb
Rate-Distortion Parameters	$D_0 = 1.18$, $E_0 = 0.67$, $\theta_0 = 858$
Video Pixel Bit-Depth	$p = 8$
Fading Threshold Step	$\boldsymbol{stp}_\beta = \{0.5, 0.01\}$
Incoming Packet Rate Step	$\boldsymbol{stp}_\lambda = \{0.5, 1\}$

Figure 29 consists of a streamer UAV, an interferer UAV, and 8 ground nodes, where the streamer and interferer UAVs stream video to their associated ground nodes.

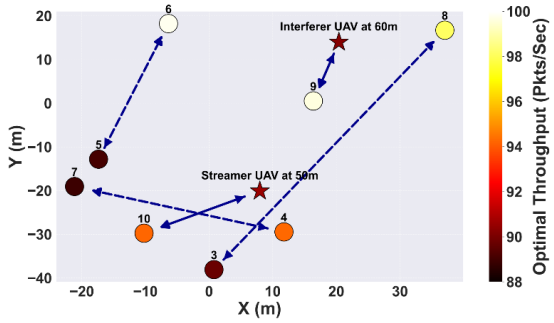

Figure 29. Nodes distribution with optimal expected throughput by DTC.

For the DTC algorithm, researchers presented detailed results showing how the optimal expected throughput and optimal channel fading threshold changed with varying SINR thresholds, number of sub-channels, and different transmission policies. This also depicted the behavior of packet loss probabilities throughout the DTC algorithm iterations.

For the JDVT-EC algorithm, the team provided comprehensive results for PSNR, channel fading threshold, and video encoding rate (see for example Table 6). Individual and joint optimizations were explored, demonstrating that optimizing both the fading threshold and encoding rate led to the best results. Furthermore, researchers illustrated the impact of varying the sensitivity parameter and SINR threshold on the optimal PSNR, optimal fading threshold, and optimal encoding rate.

Table 6. PSNR and video encoding rate values achieved with different encoding schemes.

Encoding Rate	Streamer UAV	Interferer UAV	Node 3	Node 4	Node 5	Average $\mathcal{P}$
Low	38.93 - 158.08	40.67 - 203.68	38.90 - 179.36	38.92 - 191.52	40.05 - 167.20	39.49 dB
Medium	40.35 - 325.28	41.86 - 297.92	41.42 - 307.04	39.11 - 331.36	41.68 - 273.60	40.88 dB
Optimal	**40.37 - 310.08**	**42.51 - 407.36**	**41.70 - 373.92**	**39.50 - 279.68**	**42.62 - 410.40**	**41.34** dB
High	37.00 - 431.68	42.34 - 443.84	41.30 - 425.60	35.66 - 407.36	42.42 - 449.92	39.74 dB

Moreover, the heatmap in Figure 30 show the spatial variations in these metrics with respect to the streamer UAV location. The numerical results confirmed the efficacy of the DTC and JDVT-EC algorithms, consistently yielding optimal results across various scenarios. Detailed results are also available in the team's research paper (Ghazikor et al., 2024b).

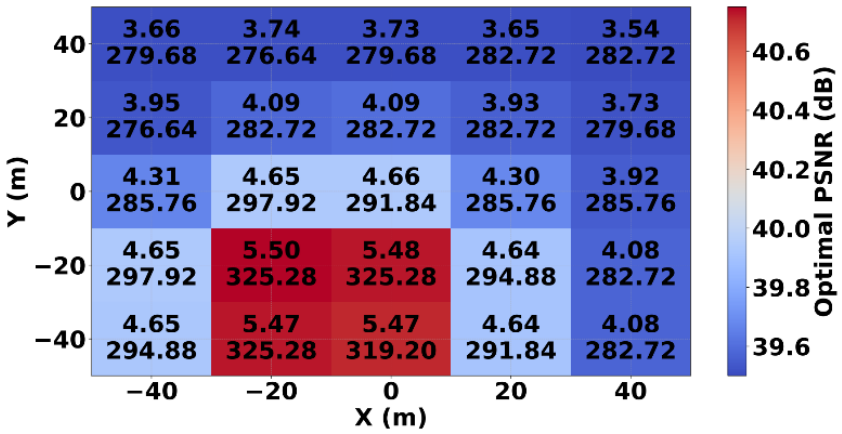

Figure 30. Optimal PSNR heatmap for different streamer UAV location by JDVT-EC.

6 SUBTASK 5: SPECTRUM MANAGEMENT FRAMEWORK FOR OPERATORS

6.1 Introduction

Continuing development in subtask 3, Figure 31 shows a simplified form of the UTM architecture, highlighting the separation between FAA and industry development and deployment responsibilities for the necessary infrastructure, services, and entities that interact within the UTM ecosystem. In this subtask, the main focus was on the hierarchical structure between multiple operators and the UAS service supplier (USS), which assists multiple operators in meeting UTM operational requirements, ensuring safe and efficient utilization of the airspace.

The concept of operations within the UTM architecture highlights the need for spectrum resources to facilitate wireless communications between UAVs, UAV operators, and the USS network. Due to the proliferation of new wireless services and the demand for higher data rates, there are spectrum shortages to support various services. Therefore, it is essential to develop dynamic spectrum sensing, inference, and sharing solutions for UAV operations in existing licensed and unlicensed spectrum (Rimjha and Trani, 2021).

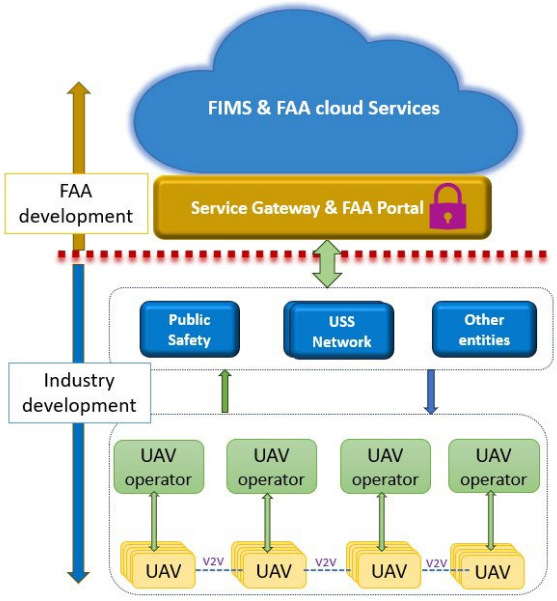

Figure 31. Simplified UTM architecture showing the separation between different entities.

There exists a multitude of prior works on spectrum management frameworks for ground users that propose deep learning-based wideband spectrum sensing to dynamically detect "spectrum holes" (Ahmad et al., 2020; Cui et al., 2020). Few works propose reinforcement learning (RL) techniques for spectrum sharing, assuming that spectrum sensing results are readily available (Nguyen et al., 2018). While these data-driven spectrum management frameworks for ground users are available, they are not directly applicable for UTM-enabled UAV operations, due to several factors, such as the widely different wireless channel models and the overall system architecture. In the context of UAV spectrum sharing systems, spatial spectral sensing (SSS) based methods are developed for efficient spectrum sharing policies for UAV communications aimed at improving the overall spectral efficiency (SE) (Kakar and Marojevic, 2017; Shang et al., 2020). However, the SSS models do not consider the spectrum usage pattern of users under realistic scenarios (e.g., ignoring the I/Q level samples), and/or they consider only a single primary user (PU) or secondary user (SU). Moreover, the problem of joint multi-channel wideband spectrum sensing and scheduling among several SUs has not been fully investigated.

In this subtask, the researchers proposed a unified and data-driven spectrum sensing and scheduling framework to enable UAVs to effectively share the spectrum with existing primary users. At the spectrum sensing stage, it is noted that the inherent hierarchical nature of the UTM architecture with USS (shown in Figure 31) is a good match for federated learning (FL)-based model training, which achieves spectrum sensing. Specific to the spectrum sensing stage, an FL-based cooperative wideband spectrum sensing across multiple UAVs was proposed. Researchers developed a multi-label classification framework to identify spectrum holes based on the observed I/Q samples. Each UAV trains their respective local models using the locally collected datasets and transmits the local model parameters to the central server. Furthermore, the team proposed a novel proportional weighted federated averaging (pwFedAvg) method that incorporates the power

level received at each UAV into the FL aggregation algorithm, thereby integrating the dataset generation plane with the FL model training plane, as shown in Figure 32.

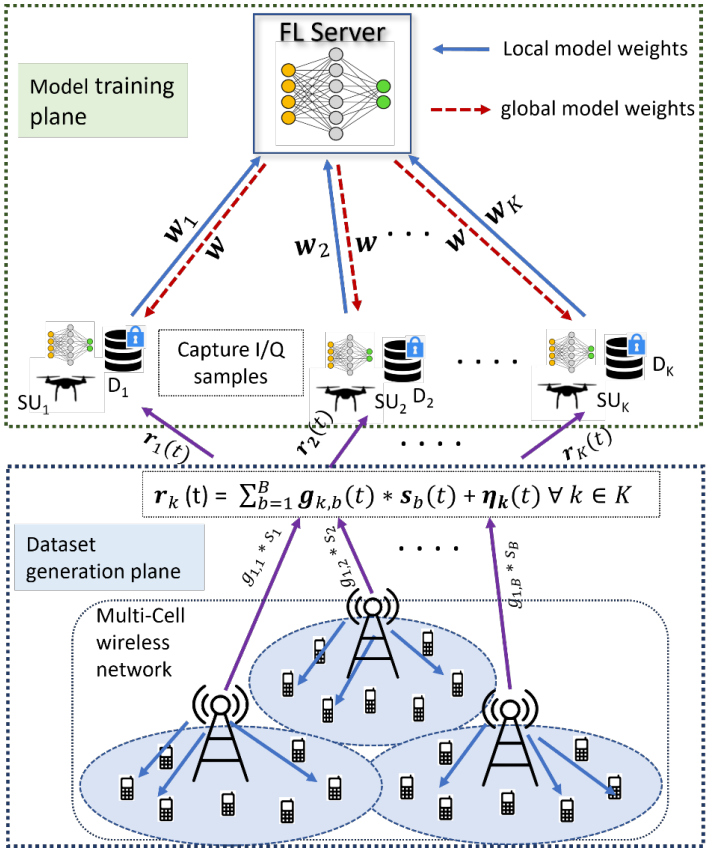

Figure 32. Envisioned FL system model in a multi-cell wireless network with multiple UAVs.

Given the simplified UTM architecture, and the basic principles of FL, researchers envision two scenarios for deploying FL-based spectrum sensing in the context of UTM architecture. These two cases are shown in Figure 33. In scenario 1, each UAS operator has its own FL Server, while in scenario 2 all operators are coordinated by a central FL server (perhaps, one per USS). Given the privacy-preserving nature of FL-based machine learning solutions, different operators do not share any raw wireless/spectrum usage data with other operators. Rather, only ML model parameters are aggregated at the FL server.

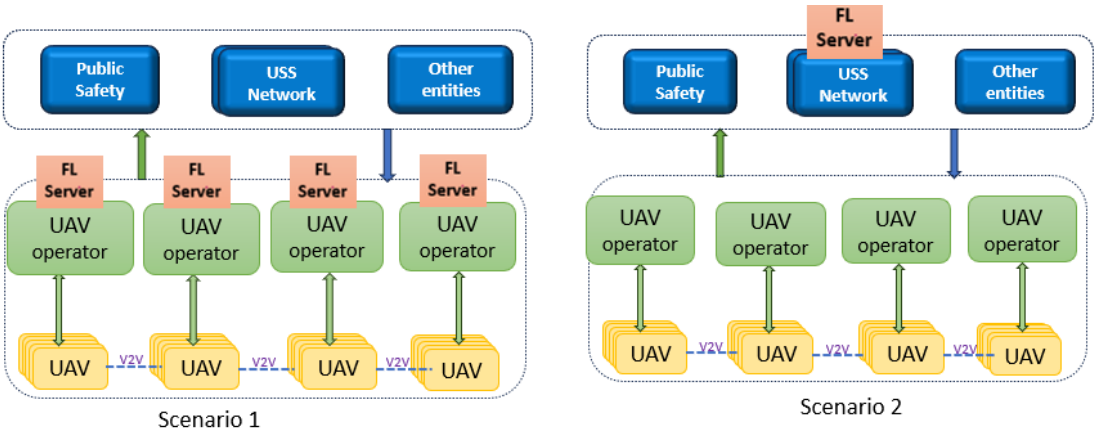

Figure 33. Envisioned FL scenarios that can be integrated with UTM architecture.

6.2 Methods

6.2.1 Proposed FL-based Model for Spectrum Sensing

An assumption made is that each UAV receives signals from more than one base-station (BS) due to the fact that they operate at higher altitudes, which increases the chances of signal reception from multiple BSs, as shown in Figure 32. Furthermore, it is assumed that the cell bandwidth W is partitioned into M orthogonal sub-channels. Then the total transmitted signal from a BS b across M orthogonal sub-channels at any time t can be represented by the superposition principle as follows:

$$s_b(t) = \sum_{m=1}^{M} I_{b,m}(t)\, v_{b,m}(t), \forall b \in \mathcal{B}, \tag{6.1}$$

where $\mathrm{I_{b,m}(t)} = 1$ if the m-th sub-channel of BS b is occupied at time t, and 0 otherwise. Moreover, $\mathrm{v}_{b,m}(\mathrm{t})$ represents the waveform on the m-th sub-channel. As a result, $\mathrm{s_b(t)}$ is the total transmitted baseband waveform at each BS. Each UAV k then receives the wideband signal from multiple BSs in a multi-path propagation environment, which can be expressed as follows:

$$r_{\boldsymbol{k}}(t) = \sum_{b=1}^{B} \boldsymbol{g}_{k,b}(t) * \boldsymbol{s}_b(t) + \boldsymbol{\eta}_k(t), \forall k \in \mathcal{K}, \tag{6.2}$$

where $\boldsymbol{g}_{k,b}(t)$ represents the multi-path channel between BS b and UAV k and $\boldsymbol{\eta}_k(t)$ denotes the thermal noise signal observed at UAV k. Therefore, the signal-to-noise ratio observed at UAV k can be written as follows:

$$\mathrm{SNR}_k(t) = \frac{\left|\left|\sum_{b=1}^{B} \boldsymbol{g}_{k,b}(t) * \boldsymbol{s}_b(t)\right|\right|^2}{\sigma_k^2(t)}, \forall k \in \mathcal{K}, \tag{6.3}$$

where $\sigma_k^2(t)$ represents the noise variance observed at UAV *k* at time *t*. $P_k(t)$ is used to denote the total power received in UAV *k* at time *t*, which is directly proportional to the signal generated as defined in Eq. (6.1). $P_k(t)$ will be used for proportional weight scaling in FL training.

To train the DNN models for predicting spectrum holes using raw I/Q samples, it has been shown that the characteristics of the wireless signal can be captured by observing only a portion of the signal waveform (Chintareddy et al., 2023; Uvaydov et al., 2021). Hence, from the received baseband signal $\boldsymbol{r_k}(t)$, capture *J* I/Q samples are captures and stored locally. Therefore, the samples from baseband waveform collected at UAV *k* are represented as $\boldsymbol{R_k}(t)$ given as follows:

$$\boldsymbol{R}_k(t) = \widetilde{\boldsymbol{R}}_{\boldsymbol{k}}(t) + +\widetilde{\boldsymbol{\eta}}_{\boldsymbol{k}}(t), \forall k \in \mathcal{K} \tag{6.4}$$

where $\widetilde{\boldsymbol{R}}_{\boldsymbol{k}}(t)$ represents the *J* I/Q samples from the first term in Eq. (6.2) and the second term represents *J* complex Gaussian noise samples. In addition to the I/Q samples, the true labels are stored for channel occupancy at each UAV *k* at time *t*. The channel occupancy vector $\boldsymbol{h}_k(t)$ is an *M*-dimensional vector, with each index indicating if a sub-channel *m* is occupied or free at time *t* and can be computed as follows:

$$h_{k,m}(t) = \begin{cases} 1, & \sum_{b=1}^{B} I_{b,m}(t) \ \geq \ 1; \\ 0, & Otherwise. \end{cases} \tag{6.5}$$

Note that $\boldsymbol{h}_k(t)$ observed at time *t* would be the true label corresponding to the wideband received signal $\boldsymbol{r_k}(t)$.The channel occupancy would remain unchanged for the stored *J* I/Q samples $\boldsymbol{R_k}(t)$. $(\boldsymbol{R_k}(t), \boldsymbol{h}_k(t))$ is stored as an input-output pair that will be used for the training of the FL model. For the sake of simplicity of notation, the input-output pair is represented as $(\boldsymbol{R_k}, \boldsymbol{h}_k)$. Note that for each *M*-dimensional channel occupancy vector $\boldsymbol{h}_k$, the input-output pair is treated as one data sample and the total I/Q dataset collected at UAV *k* is denoted as follows:

$$D_k = \left\{(R_k^1, h_k^1), (R_k^2, \boldsymbol{h}_k^2), \ldots \left(R_k^{|D_k|}, h_k^{|D_k|}\right)\right\}, \tag{6.6}$$

where $|\boldsymbol{D}_k|$ represents the total number of samples in the UAV *k*. These local datasets are used in FL-based training for spectrum hole detection.

In the FL setting, each UAV *k* trains a local wideband spectrum sensing model whose parameters are denoted by ω_k. Hence, the primary objective of the local model is to find a mathematical function $f(\boldsymbol{\omega}_k, \boldsymbol{R}_k)$, that maps input I/Q samples $\boldsymbol{R}_k$ to $\boldsymbol{h}_k$, i.e.,

$$f(\omega_k, R_k): R_k \rightarrow h_k \tag{6.7}$$

To this end, using the raw I/Q samples$\boldsymbol{R}_k$ each UAV *k* trains a local model that detects vacant sub-channels, such that the local loss function $L_k(\omega)$ minimizes the error between the true labels $\boldsymbol{h}_k$ and the predicted labels $\widehat{h_k}$, as defined below:

$$L_k(\boldsymbol{\omega}) \triangleq \frac{1}{|\boldsymbol{D_k}|}\sum_{i=1}^{|\boldsymbol{D_k}|} l\big(f\big(\boldsymbol{\omega}_k, \boldsymbol{R}_k^i\big); \boldsymbol{h}_k^i\big), \tag{6.8}$$

where $l(.)$ is the loss function for computing the prediction loss in the supervised machine learning setting. Furthermore, $f(.,.)$ represents the predicted label for the sample $(\boldsymbol{R}_k^i, \boldsymbol{h}_k^i)$ and $\boldsymbol{\omega}_k$ represents the local model parameters during training.

Given the system model, a framework for wideband spectrum sensing is introduced where multiple UAVs collaboratively participate in the FL. In such a distributed learning environment, the aim is to learn a global statistical model at the central server. Given that each UAV k trains a local model to identify the spectrum holes by minimizing the local loss function $L_k(\boldsymbol{\omega})$, in the context of FL, the aggregated global loss function $\mathrm{L}(\omega)$ should be minimized, as follows:

$$\min_{\boldsymbol{\omega}} \left\{ L(\boldsymbol{\omega}) \triangleq \sum_{k=1}^{K} \frac{|\boldsymbol{D}_k|}{D} L_k(\boldsymbol{\omega}) \right\}, \tag{6.9}$$

where $\mathrm{D} = \sum_{\mathrm{k}=1}^{\mathrm{K}} |\mathrm{D}_k|$ is the total size of data samples across the UAVs.

To solve the global loss function Eq. (6.9), the authors in (McMahan et al., 2023) proposed FedAvg, an iterative aggregation algorithm where the global model aggregates the local model gradients and redistributes the global model weights to the local models. However, when the datasets of each UAV k are of equal size, FedAvg assigns equal scaling factor of $\frac{1}{\mathrm{K}}$ for all local gradients. However, in the considered multi-cell environment, the signal received at different UAV locations experiences different channel conditions, and the signal power received at different locations varies significantly. Hence, by assigning equal scaling weights for the local model gradients, the performance metrics at UAV locations with strong signal deteriorate. To compensate for this effect and improve performance at locations that receive better signal power, a proportional weight scaling aggregation method for FL (pwFedAvg) is proposed that intuitively assigns smaller weights to UAVs with lower received signal power (i.e., poor channel conditions), and larger weights to those UAVs with higher received signal power.

Using the pwFedAvg, the central server aggregates the local gradients by assigning a weight proportional to their received signals as follows:

$$\nabla L(\omega^t) = \sum_{k=1}^{K} \frac{\alpha_k^t}{\alpha^t} \nabla L_k(\omega_k^t; \xi_k^t), \tag{6.10}$$

where $\alpha_{\mathrm{k}}^{\mathrm{t}} = \sqrt{\overline{P}_k^t}$ and $\alpha^{\mathrm{t}} = \sum_{k=1}^{K} \sqrt{\overline{P}_k^t}$. Here, $\overline{P}_k^t$ represents the average received signal power at UAV k for the batch of samples $\boldsymbol{\xi}_k^t$. Note that during the FL training process at time t, $\boldsymbol{\omega}_k^t$ and $\boldsymbol{\omega}^t$denote the local and global model weights, respectively. Upon computing the global model gradient based on Eq. 6.10, the global model weights are updated as follows:

$$\omega^{t+1} = \boldsymbol{\omega}^t - \gamma^t \nabla L(\boldsymbol{\omega}^t), \tag{6.11}$$

where γ^t is the learning rate of the global model. The updated global model weights are sent to the clients to update their local model weights. Once the training process is completed, all UAVs have an updated global model that predicts spectrum *holes*. However, it is inevitable that different UAVs located at different places perform differently. To effectively estimate spectrum *holes* and manage the spectrum efficiently, a spectrum fusion model is proposed that fuses or aggregates all the spectrum holes predicted from different UAVs. The spectrum fusion is assumed to be part of the central server within the UTM ecosystem. The overall process of FL-based model training using the pwFedAvg approach is outlined in Algorithm shown in Figure 33.

Algorithm 1 Channel-Aware FL-Based Training

Initialize the global model parameters $\boldsymbol{\omega}$ and local model $\boldsymbol{\omega_k}$, $\forall k \in \mathcal{K}$; T : Communication rounds.
for t in T **do**
  for UAV k in $\mathcal{K}$ **do**
    Choose a batch of I/Q samples $\boldsymbol{\xi}_k^t \subseteq \boldsymbol{D}_k$.
    Train the local model for E epochs.
  end for
  Send the gradients $\nabla L_k(\boldsymbol{\omega}_k^t; \boldsymbol{\xi}_k^t)$ to the central server.
  Aggregate local gradients at the server.
  Update the global model at the server.
  Update local models using the global model, i.e., $\boldsymbol{\omega}_k^{t+1} = \boldsymbol{\omega}^{t+1}$.
end for

Figure 34. Algorithm for channel-aware FL-based training.

6.3 Results

As previously stated, the researchers modelled wideband spectrum sensing, aiming to identify spectrum holes from the given I/Q samples as inputs to the ML model. The same evaluation scenario as in subtask 3 is used here, in which 3 UAVs in 3 different locations are emulated in simulation environment. The team used 70% of the dataset to train the model using federated learning (FL) and 30% for spectrum inference purposes. To investigate FL performance, the FedAvg algorithm was implemented, and the results are presented in Figures 34 through Figure 36. From the results, it is noted that FedAvg achieves good performance only for the UAV locations 2 and 3 (Figure 35 (a) and Figure 36 (a)). Given the heterogeneous dataset collected at different UAV locations, the overall performance of FedAvg is limited by the UAV(s) that performs the worst. This is because FedAvg scales the weights of all local models equally. To reduce the impact of UAV locations with poor performance, the proposed pwFedAvg algorithm scales the weights of local models according to the received signal power. As shown in Figure 35

(b) and Figure 36 (b), the proportional weighting scheme can improve the F-1 score performance at locations 2 and 3.

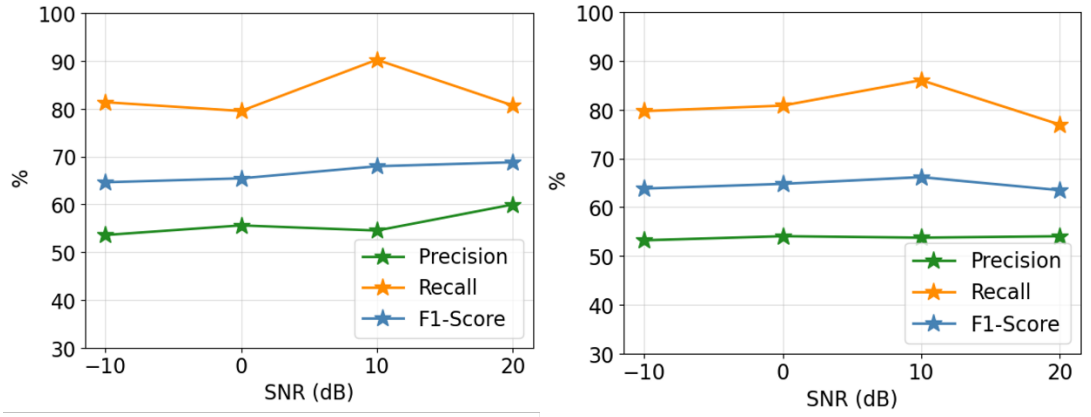

(a) FL-FedAvg: location 1 (b) FL-pwFedAvg: location 1

Figure 35. Comparison of performance metrics at location 1: (a) FL-FedAvg, (b) FL-pwFedAvg.

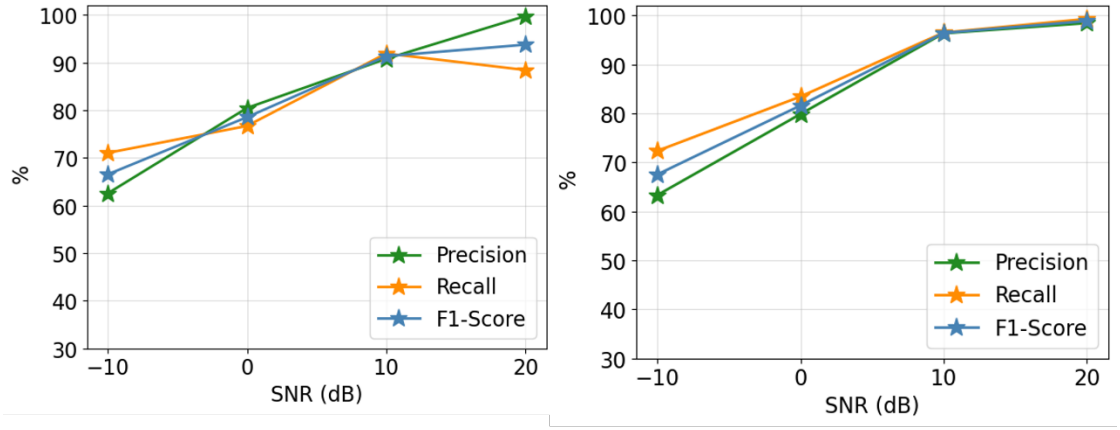

(a) FL-FedAvg: location 2 (b) FL-pwFedAvg: location 2

Figure 36. Comparison of performance metrics at location 2: (a) FL-FedAvg, (b) FL-pwFedAvg.

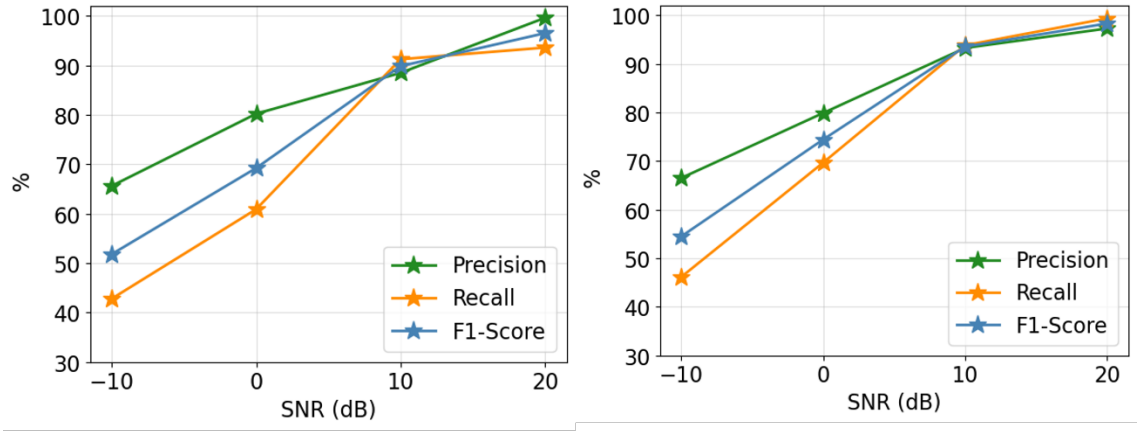

(a) FL-FedAvg: location 3 (b) FL-pwFedAvg: location 3

Figure 37. Comparison of performance metrics at location 3: (a) FL-FedAvg, (b) FL-pwFedAvg.

Additionally, centralized learning (CL) was performed as another baseline. CL is a technique in which it is assumed that all the data collected at different locations are aggregated at one central server and are readily available to train the ML model. Furthermore, to have a fair comparison, the F1-score is plotted for CL, FL-FedAvg and FL-pwFedAvg as shown in Figure 37 (a), (b), (c). With the proposed aggregating scheme (pwFedAvg), the performance metrics are improved at UAV locations 2 (Figure 37 (b)) and 3 (Figure 37 (c)), without significantly affecting location 1 (Figure 37 (a)) performance.

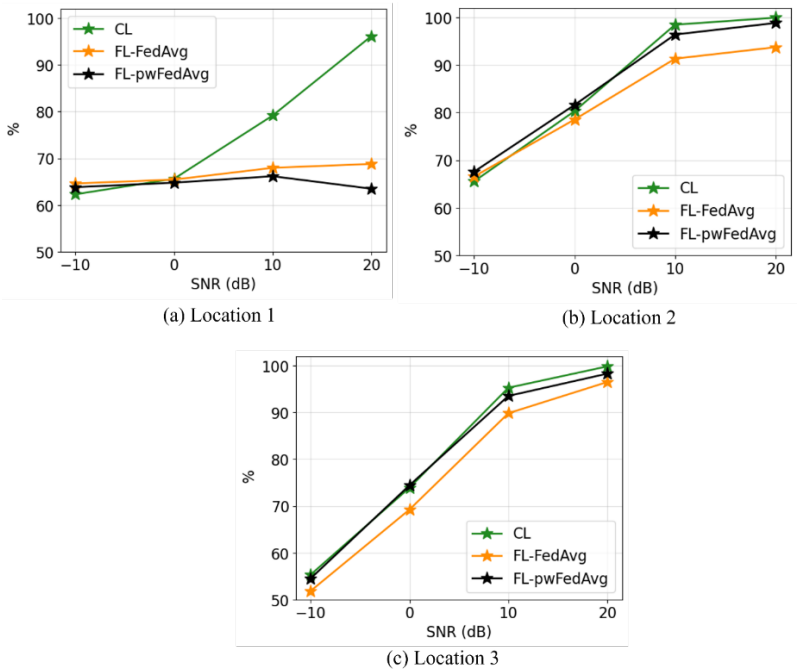

(a) Location 1 (b) Location 2

(c) Location 3

Figure 38. F1-Score comparison for CL, FL-FedAvg, FL-pwFedAvg: (a) Location1, (b) Location 2, (c) Location 3.

It is observed from the results in Figure 37 that individual sensing performance might fluctuate at different locations, in both the CL and FL settings. However, by applying fusion rules, the overall performance is significantly improved, as shown by the results in Figure 38. From these results, researchers noticed that the overall performance of all methods is significantly improved by fusion. Furthermore, the proposed pwFedAvg algorithm outperforms FedAvg, while achieving comparable results with respect to the CL method without the need to transfer all datasets to a central location.

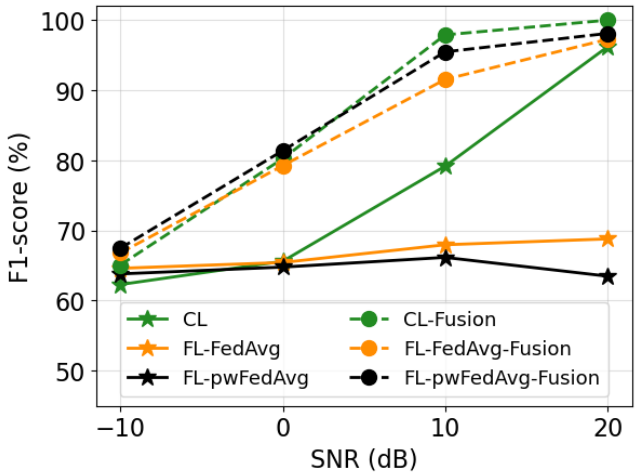

Figure 39. F1-Score comparison at location 1 with and without fusion.

7 CONCLUSION

This research on spectrum management for Unmanned Aerial Systems (UAS) in public safety and Beyond Visual Line of Sight (BVLOS) operations presents several technical findings and contributions. The study focused on several major subtasks: spectrum needs and supplies, dynamic spectrum sharing, interference analysis, and spectrum management frameworks. Each subtask provides insight into current limitations and future opportunities for UAS communication systems.

When considering spectrum demands and shortages, the projected increase in UAS density under BVLOS conditions requires more spectrum resources to enable safe and reliable operations. Both public safety and commercial UAS operations will struggle to maintain communication quality using unlicensed bands (e.g., WiFi). The use of cellular networks for BVLOS operations, while promising, is limited by bandwidth constraints and potential interference since those networks are not designed and implemented for UAS applications.

On the topic of collaborative spectrum sharing and dynamic allocation, it can be concluded that introducing collaborative spectrum sensing and ML/AI-driven solutions has proven effective in improving spectrum utilization. This research demonstrates that UAS can autonomously detect and share underutilized spectrum, so that the spectrum efficiency is enhanced. Dynamic allocation strategies using Reinforcement Learning (RL) methods such as Double Deep Q-Networks (DDQN), showed performance gains by optimizing spectrum usage across distributed UAVs.

In terms of interference mitigation in unlicensed bands and optimization of communication systems, the developed interference-aware distributed transmission control algorithms are effective to manage interference in unlicensed spectrum bands. These algorithms effectively adjusted transmission policies based on wireless channel conditions and interference levels, thereby increasing throughput and reducing message errors in UAS communications.

Federated learning (FL) frameworks were investigated to enhance spectrum management for UAS. The FL-based approaches provide a decentralized solution that maintains data privacy while improving spectrum allocation decisions. The proposed proportional weighted federated averaging (pwFedAvg) algorithm incorporates wireless channel conditions into the model aggregation process to improve the performance of standard FL models.

Despite these advancements, several key challenges remain in regard to policy and regulation, real-world validation of solutions, and infrastructure enhancement,

Current spectrum policies do not sufficiently address the specific requirements of UAS operations. The lack of dedicated spectrum for UAS operations, particularly in public safety contexts, creates a significant bottleneck. The FCC's recent NPRM and subsequent regulations on the 5030-5091 MHz band (C-band) represent a step in the right direction, but more coordinated efforts are needed to establish reliable and interference-protected spectrum access for UAS. Priority spectrum access for public safety applications should be incorporated into the regulations.

While the proposed ML/AI-driven spectrum management solutions performed well in simulations, real-world testing is required to validate their robustness, scalability, and adaptability in dynamic environments. Experimental trials in urban and rural environments, with varying levels of UAV density and spectrum availability, are essential for refining these solutions.

The use of existing cellular infrastructure for UAS communications poses potential challenges, particularly in terms of interference. Investing in communication technologies and further studies that are future-proof, such as C-band radio for licensed spectrum access for UAS, will be critical to ensuring reliable and safe BVLOS operations.

In conclusion, addressing the spectrum needs of UAS for public safety and other applications will require a combination of innovative technologies, robust policy support, and infrastructure investment. These steps are essential to unlocking the full potential of UAS in complex and high-density environments.

8 REFERENCES

Ahmad, W.S.H.M.W., Radzi, N.A.M., Samidi, F.S., Ismail, A., Abdullah, F., Jamaludin, M.Z., Zakaria, M.N., 2020. 5G Technology: Towards Dynamic Spectrum Sharing Using Cognitive Radio Networks. IEEE Access 8, 14460–14488. https://doi.org/10.1109/ACCESS.2020.2966271

Azari, M.M., Rosas, F., Chen, K.-C., Pollin, S., 2018. Ultra Reliable UAV Communication Using Altitude and Cooperation Diversity. IEEE Trans. Commun. 66, 330–344. https://doi.org/10.1109/TCOMM.2017.2746105

Berahas, A.S., Bollapragada, R., Keskar, N.S., Wei, E., 2019. Balancing Communication and Computation in Distributed Optimization. IEEE Trans. Autom. Control 64, 3141–3155. https://doi.org/10.1109/TAC.2018.2880407

Chintareddy, S.R., Roach, K., Cheung, K., Hashemi, M., 2023. Collaborative Wideband Spectrum Sensing and Scheduling for Networked UAVs in UTM Systems, in: GLOBECOM 2023 - 2023 IEEE Global Communications Conference. Presented at the GLOBECOM 2023 - 2023 IEEE Global Communications Conference, pp. 3064–3069. https://doi.org/10.1109/GLOBECOM54140.2023.10436809

Cui, J., Liu, Y., Nallanathan, A., 2020. Multi-Agent Reinforcement Learning-Based Resource Allocation for UAV Networks. IEEE Trans. Wirel. Commun. 19, 729–743. https://doi.org/10.1109/TWC.2019.2935201

FCC, 2023. FCC Starts Rulemaking on Licensed Spectrum for Unmanned Aircraft Use: https://www.fcc.gov/document/fcc-starts-rulemaking-licensed-spectrum-unmanned-aircraft-use.

Ghazikor, M., Roach, K., Cheung, K., Hashemi, M., 2024a. Interference-Aware Queuing Analysis for Distributed Transmission Control in UAV Networks, in: ICC 2024 - IEEE International Conference on Communications. Presented at the ICC 2024 - IEEE International Conference on Communications, IEEE, Denver, CO, USA, pp. 4524–4529. https://doi.org/10.1109/ICC51166.2024.10623099

Ghazikor, M., Roach, K., Cheung, K., Hashemi, M., 2024b. Channel-Aware Distributed Transmission Control and Video Streaming in UAV Networks. https://doi.org/10.48550/arXiv.2408.01885

Ghazikor, M., Roach, K., Cheung, K., Hashemi, M., 2023. Exploring the Interplay of Interference and Queues in Unlicensed Spectrum Bands for UAV Networks, in: 2023 57th Asilomar Conference on Signals, Systems, and Computers. Presented at the 2023 57th Asilomar Conference on Signals, Systems, and Computers, IEEE, Pacific Grove, CA, USA, pp. 729–733. https://doi.org/10.1109/IEEECONF59524.2023.10476884

Guan, Z., Melodia, T., Scutari, G., 2016. To Transmit or Not to Transmit? Distributed Queueing Games in Infrastructureless Wireless Networks. IEEEACM Trans. Netw. 24, 1153–1166. https://doi.org/10.1109/TNET.2015.2412116

Hasselt, H. van, Guez, A., Silver, D., 2016. Deep reinforcement learning with double Q-Learning, in: Proceedings of the Thirtieth AAAI Conference on Artificial Intelligence, AAAI'16. AAAI Press, Phoenix, Arizona, pp. 2094–2100.

ITU-R, 2009. Report ITU-R M.2171: https://www.itu.int/en/ITU-R/space/snl/Documents/R-REP-M.2171-2009-PDF-E.pdf.

Kakar, J., Marojevic, V., 2017. Waveform and spectrum management for unmanned aerial systems beyond 2025, in: 2017 IEEE 28th Annual International Symposium on Personal, Indoor, and Mobile Radio Communications (PIMRC). Presented at the 2017 IEEE 28th Annual International Symposium on Personal, Indoor, and Mobile Radio Communications (PIMRC), pp. 1–5. https://doi.org/10.1109/PIMRC.2017.8292533

Kakar, J.A., 2015. UAV Communications: Spectral Requirements, MAV and SUAV Channel Modeling, OFDM Waveform Parameters, Performance and Spectrum Management (Thesis). Virginia Tech.

Khan, N., Ahmad, A., Wakeel, A., Kaleem, Z., Rashid, B., Khalid, W., 2024. Efficient UAVs Deployment and Resource Allocation in UAV-Relay Assisted Public Safety Networks for Video Transmission. IEEE Access 12, 4561–4574. https://doi.org/10.1109/ACCESS.2024.3350138

Kim, M., Lee, J., 2019. Impact of an Interfering Node on Unmanned Aerial Vehicle Communications. IEEE Trans. Veh. Technol. 68, 12150–12163. https://doi.org/10.1109/TVT.2019.2949345

Kopardekar, P., Rios, J., Prevot, T., Johnson, M., Jung, J., Robinson, J.E., 2016. Unmanned Aircraft System Traffic Management (UTM) Concept of Operations. Presented at the AIAA AVIATION Forum and Exposition, Washington, DC.

McMahan, H.B., Moore, E., Ramage, D., Hampson, S., Arcas, B.A. y, 2023. Communication-Efficient Learning of Deep Networks from Decentralized Data.

Muruganathan, S.D., Lin, X., Maattanen, H.-L., Sedin, J., Zou, Z., Hapsari, W.A., Yasukawa, S., 2021. An Overview of 3GPP Release-15 Study on Enhanced LTE Support for Connected Drones. IEEE Commun. Stand. Mag. 5, 140–146. https://doi.org/10.1109/MCOMSTD.0001.1900021

Nguyen, H.Q., Nguyen, B.T., Dong, T.Q., Ngo, D.T., Nguyen, T.A., 2018. Deep Q-Learning with Multiband Sensing for Dynamic Spectrum Access, in: 2018 IEEE International Symposium on Dynamic Spectrum Access Networks (DySPAN). Presented at the 2018 IEEE International Symposium on Dynamic Spectrum Access Networks (DySPAN), pp. 1–5. https://doi.org/10.1109/DySPAN.2018.8610402

NTIA, 2024. National Spectrum Strategy Implementation Plan: https://www.ntia.gov/sites/default/files/publications/national-spectrum-strategy-implementation-plan.pdf.

NTIA, 2021. NTIA Frequency Allocation for 5030-5250 MHz: https://www.ntia.doc.gov/files/ntia/publications/compendium/5030.00-5250.00-02092021.pdf.

Rimjha, M., Trani, A., 2021. Urban Air Mobility: Factors Affecting Vertiport Capacity, in: 2021 Integrated Communications Navigation and Surveillance Conference (ICNS). Presented at the 2021 Integrated Communications Navigation and Surveillance Conference (ICNS), pp. 1–14. https://doi.org/10.1109/ICNS52807.2021.9441631

Shang, B., Marojevic, V., Yi, Y., Abdalla, A.S., Liu, L., 2020. Spectrum Sharing for UAV Communications: Spatial Spectrum Sensing and Open Issues. IEEE Veh. Technol. Mag. 15, 104–112. https://doi.org/10.1109/MVT.2020.2980020

Sutton, R.S., Barto, A.G., 2018. Reinforcement learning: an introduction, Second edition. ed, Adaptive computation and machine learning series. The MIT Press, Cambridge, Massachusetts.

Tian, J., Zhang, H., Wu, D., Yuan, D., 2016. Interference-Aware Cross-Layer Design for Distributed Video Transmission in Wireless Networks. IEEE Trans. Circuits Syst. Video Technol. 26, 978–991. https://doi.org/10.1109/TCSVT.2015.2430611

Uvaydov, D., D'Oro, S., Restuccia, F., Melodia, T., 2021. DeepSense: Fast Wideband Spectrum Sensing Through Real-Time In-the-Loop Deep Learning, in: IEEE INFOCOM 2021 - IEEE Conference on Computer Communications. Presented at the IEEE INFOCOM 2021 - IEEE Conference on Computer Communications, pp. 1–10. https://doi.org/10.1109/INFOCOM42981.2021.9488764

Zhang, X., Shin, K.G., 2012. E-MiLi: Energy-Minimizing Idle Listening in Wireless Networks. IEEE Trans. Mob. Comput. 11, 1441–1454. https://doi.org/10.1109/TMC.2012.112